Non-nucleophilic base promoted synthesis of azo-linked oxazolone-pyrazole hybrids: Antimicrobial, antitubercular, anticancer evaluations and *in-silico* modeling insights

Bonny Y. Patel [a,*], Vidhi Joshi [b], Sangeetha Subramanian [c], Gopal Italiya [c],
Prasanna Srinivasan Ramalingam [c], Sivakumar Arumugam [c], Sanjay D. Hadiyal [d],
Al-Anood Mohamed Al-Dies [e]

[a] *School of Science, Department of Chemistry, RK University, Rajkot 360020, Gujarat, India*
[b] *Department of Chemistry, B.V. Shah (Vadi-Vihar) Science College, C.U. Shah University, Wadhwan City, Surendranagar 363001, Gujarat, India*
[c] *School of Biosciences and Technology (SBST), Vellore Institute of Technology, Vellore, Tamil Nadu 632014, India*
[d] *Department of Chemistry, Atmiya University, Rajkot 360005, Gujarat, India*
[e] *Chemistry Department, Umm Al-Qura University, Al-Qunfudah University College, Saudi Arabia*

ARTICLE INFO

ABSTRACT

Ten new non-nucleophilic base (DBU) catalyzed oxazolone-bearing pyrazole derivatives were created to treat infectious diseases caused by bacterial, mycobacterial strains, and cancerous cell lines. Compounds **7b** and **7c** showed excellent antibacterial and antifungal activity. Compound **7b** was highly effective against *M. tuberculosis* H37Rv, with a MIC of 0.06 μg/mL and significant binding affinities to AcrB of *E. coli* (−12 Kcal/mol), TriABC of *P. aeruginosa* (−12.5 Kcal/mol), and MepR of *S. aureus* (−10.6 Kcal/mol). Based on the findings, compounds **7b**, **7c**, and **7e** exhibit proficient binding affinity with two essential targets, namely Enoyl-[acyl-carrier-protein] reductase and Topoisomerase I, of *M. tuberculosis*. Compound **7b** showed superior cytotoxic activity against all cancer types except leukemia with GI_{50} values of 1.26–1.83 μM and LC_{50} values of 5.36–7.88 μM. Compound **7a** demonstrated remarkable anticancer activity against colon, melanoma, ovarian, renal, and breast cancer cell lines with GI_{50} values of 1.60–2.55 μM.

Introduction

There is a growing concern about pathogens becoming resistant to antimicrobial drugs, which are used to treat many infections. To combat this, it is important to improve the use of existing drugs and develop new, effective antimicrobials [1]. Furthermore, as drug resistance continues to increase, significant effort and investment will be needed to eliminate tuberculosis disease [2]. Heterocycles that exclusively contain nitrogen and oxygen are of particular interest, as they are used in the production of both natural and synthetic products, and are commonly found in modern drug discovery [3]. Consequently, the development of new methods for synthesizing heterocyclic compounds has become a major area of research interest for chemists, pharmacists, and scientists [4]. Oxazolones, for instance, have been identified as having diverse applications due to their varied properties. Heterocyclic compounds like oxazolone or azalactone have played a vital role since 1883 in creating various micro-scale chemical molecules including amino alcohols, amino acids, vitamins, peptides, and poly-functional compounds [5]. These compounds exhibit various biological and photophysical properties, including antimicrobial, antitubercular, anti-inflammatory, anticancer, antioxidant, anticonvulsant, sedative, cardiotonic, photoswitching, fluorescence, and insecticidal activity [6–9]. The Erlenmeyer azlactone synthesis is commonly used to create oxazolone, and this traditional method has been utilized to synthesize the key aldehyde, 3-((5-oxo-2-phenyloxazol-4(5*H*)-ylidene)methyl)benzaldehyde (3). Previously, the same molecule had been synthesized using a modified method involving ionic liquid [10]. Additionally, pyrazoles have gained attention for their chemical and biological activity, acting as protein glycation inhibitors, antibacterial, antioxidant, antiviral, antifungal, anticancer, antidepressant, and anti-inflammatory agents [11–13]. The researchers have developed the 5-amino-pyrazole-4-carbonitrile nucleus using various green and conventional methods.

However, the environmentally friendly protocols have been selected under different basic catalytic conditions for this study [14].

Azo dyes are the most commonly used dyes, accounting for over 60 % of total dyes used. A staggering 70 % of all azo dyes used in commercial sectors are of the azo variety. These dyes are primarily synthetic colorants, but also exhibit various biological activities, including antimicrobial, antiviral, anticonvulsant, antidiabetic, anti-inflammatory, antitubercular, anticancer, and antioxidant properties [15–17]. Moreover, they find wide applications in non-biological industries such as cosmetics, textiles, paper production, printing, as well as in high-tech fields such as laser material, xerography and holographic data storage [18,19]. The coupling of polycyclic azo bridge with hetero aromatic or organic molecules have diverse biological activities and can be used in the fields of medicinal chemistry. Our research and literature reports indicate that combining two heterocyclic moieties in a single molecular framework can lead to the creation of more potent lead candidates [20–25]. Thus, this study focuses on designing novel motifs with oxazolone and pyrazole mono-azo derivatives through a bioinformatics study to determine their biological significance.

Results and discussion

Chemistry

The synthesis of our designed molecules requires a specific starting material, which is prepared as outlined in Scheme 1. The 3-((5-oxo-2-phenyloxazol-4(5H)-ylidene)methyl)benzaldehyde (3) in high yields has been obtained using the Erlenmeyer–Plöchl azlactone reaction approach from isophthalaldehyde (1) and hippuric acid (2) with sodium acetate as a catalyst. The novel aldehyde (3) then cyclized to a 1H-pyrazole intermediate using malononitrile (4) and phenylhydrazine (5) using basic catalysts. After experimentation, DBU was identified as the most effective catalyst for forming the primary amine pyrazole intermediate. (6). Next, the diazotization reaction using corresponding phenol derivatives was performed with intermediate (6) at 0–5 °C to obtain various azo dye analogs (7a–j) with high yields ranging from 75 % to 92 %. The synthetic route for the preparation of 5-(2-(aryl)diazenyl)-3-(3-(5-oxo-2-phenyloxazol-4(5H)-ylidene)methyl)phenyl)-1-phenyl-1H-pyrazole-4-carbonitrile (7a–j) is illustrated in Scheme 2 [26].

The synthesis of a new intermediate compound, 5-amino-3-(3-((5-oxo-2-phenyloxazol-4(5H)-ylidene)methyl)phenyl)-1-phenyl-1H-pyrazole-4-carbonitrile (6), has been attempted under various reaction conditions. The reaction was tested using different polar protic solvents and basic catalysts with conventional heating. It was observed that the solvent system used had a significant impact on the reaction yield and completion time. When potassium carbonate was used as a catalyst, the yield was 56 % in 210 min (Entry 5), while Triethyl amine (TEA) as a catalyst resulted in a yield of 63 % in 180 min (Entry 4) when used in a 50 % v/v ethanol–water mixture. On the other hand, dichloromethane only produced trace amounts of the product after more than 245 min of reaction time with both catalysts. It observed that DBU and DABCO are effective catalysts for obtaining a good yield. In comparing the yield and reaction time, the non-nucleophilic base DBU resulted in the highest yield of 93 % with a reaction time of only 100 min. This occurred in a solvent system consisting of 50 % ethanol and 50 % water (Entry 2). In contrast, the nucleophilic base DABCO produced a comparably lower yield and required more time for the reaction (Entry 3). The reaction was also attempted without any catalyst in the same solvent systems to confirm if any product formation would occur, but unfortunately, no results were obtained (Entry 1). A similar reaction condition has been reported in the literature for the formation of the pyrazole nucleus using a DABCO catalyst with simple aldehyde derivatives. However, DBU was more effective when used with 3-((5-oxo-2-phenyloxazol-4(5H)-ylidene)methyl)benzaldehyde as the starting reagent [31]. The optimized results have been summarized in Table 1.

Antimicrobial evaluation

The addition of different phenol substitutions to the azo group may be the reason for the variety in antimicrobial activity. When the azo group was combined with a Naphthol group substitution, compounds 7b (1-Naphthol) and 7c (2-Naphthol) displayed excellent antibacterial and antifungal activity, similar to standard drugs. Compound 7b, substituted with 1-Napththol, showed strong and equal activity against *E. coli* (25 μg/mL), *S. aureus* (50 μg/mL), and *S. pyogenes* (50 μg/mL). Compound 7c demonstrated significant antimicrobial efficacy against gram-negative strain *P. aeruginosa* and *A. clavatus* fungus. Additionally, compound 7e (3-NO₂), which was substituted with EWGs, exhibited moderate antimicrobial activity against *P. aeruginosa* and *A. niger* microbes. However, other synthesized compounds had only mild or no activity against the selected microorganisms (Table 2) [27].
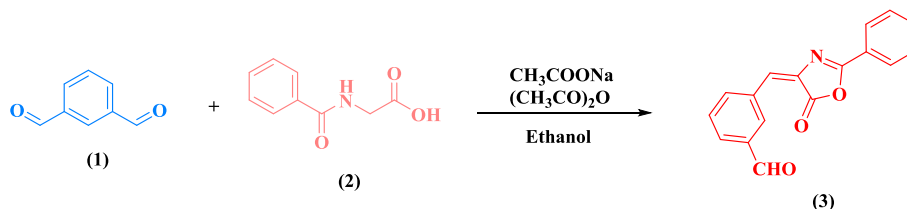
Antitubercular evaluation

During the analysis of antitubercular activity, it was found that compounds 7b (1-Naphthol), 7c (2-Naphthol), and 7e (3-Nitrophenol) displayed significant % inhibition and MIC values (Table 3). Among the three, 7b was found to be less toxic than 7c and 7e. In the primary *in-vitro* screening, both 7b and 7c were successful in suppressing *M.tb.* within the range of 89–95 %. In the secondary stage screening, compound 7b was found to suppress Mtb (94 %) with a MIC of 0.06 μg/mL, similar to the reference standard isoniazid. Therefore, the newly synthesized compound 7b with a MIC ≤ 1 μg/mL (SI = 166.66) shows promise as a bioactive lead and should undergo further analysis in the future [27].

Molecular interactions of hit compounds with targets

The compounds were docked against the crucial targets of pathogenic bacteria, fungi and *M. tuberculosis* as well as their binding affinities are showed in Tables 4 and 5. Generally, the compounds showing higher negative binding energies are highly considered as hot compounds because of their potential binding affinities towards the site of the target protein [28]. The hydrogen bonds (H-bonds) are capable of displacing the excess water molecules bound on the target protein surface when introduced in the bulk solvent environment [29].

The H-bond interactions and other interactions which include the Vander wall's force, hydrophobic interactions and electrostatic interactions between the antibacterial, antifungal, anti-tuberculosis

Scheme 1. Synthetic path of compound 3.

Where R: [a] -C$_6$H$_5$O (Phenol) [b] -C$_{10}$H$_7$O (1-Naphthol)
[c] -C$_{10}$H$_7$O (2-Naphthol) [d] -C$_6$H$_4$NO$_3$ (2-Nitrophenol)
[e] -C$_6$H$_4$NO$_3$ (3-Nitrophenol) [f] -C$_6$H$_4$NO$_3$ (4-Nitrophenol)
[g] -C$_6$H$_5$O$_2$ (Resorcinol) [h] -C$_6$H$_5$O$_2$ (Pyrocatechol)
[i] -C$_6$H$_6$NO (4-Aminophenol) [j] -C$_{15}$H$_{15}$O$_2$ (Bisphenol-A)
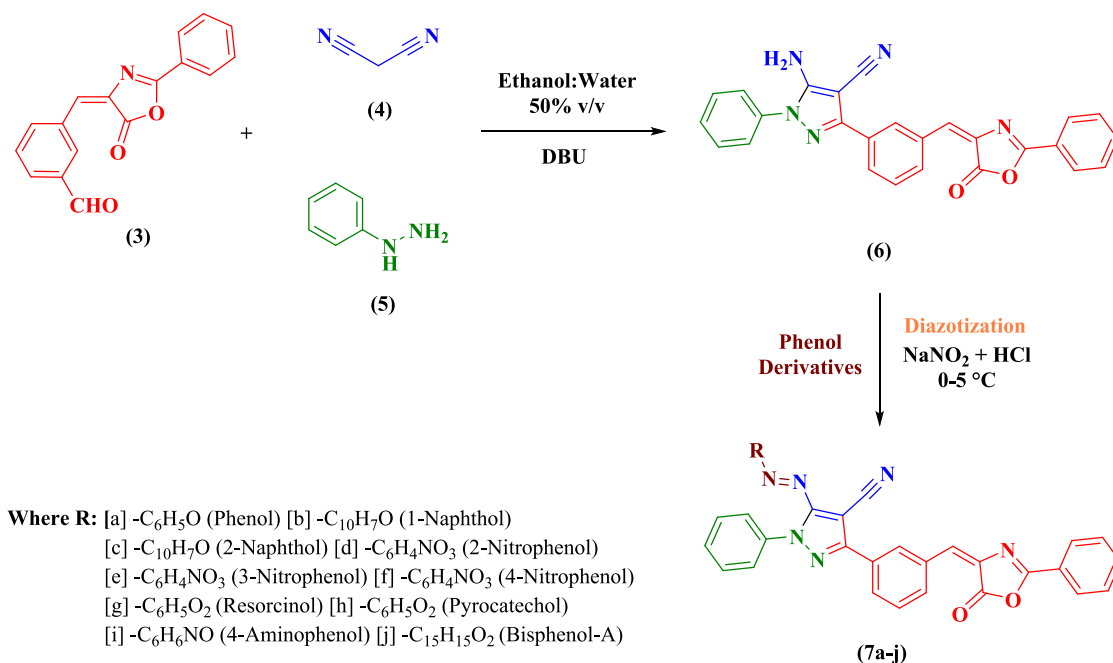
Scheme 2. Synthetic pathway for the synthesis of compounds **7a–j**.

Table 1
Optimization of compound **6** under diverse conditions.

Entry	Catalyst	Solvent system	Time (Min)	Yield (%)
1	No catalyst	Dichloromethane	No reaction	NIL
		Methanol	No reaction	NIL
		Ethanol	No reaction	NIL
		Ethanol: water	No reaction	NIL
2	DBU[a]	Dichloromethane	185	70
		Methanol	170	72
		Ethanol	160	78
		Ethanol: water	**90**	**93**
3	DABCO[b]	Dichloromethane	205	61
		Methanol	185	64
		Ethanol	175	71
		Ethanol: water	130	80
4	TEA[c]	Dichloromethane	245	Trace
		Methanol	220	40
		Ethanol	205	45
		Ethanol: water	180	63
5	K$_2$CO$_3$	Dichloromethane	<300	Trace
		Methanol	280	39
		Ethanol	220	42
		Ethanol: water	210	56

[a] DBU = 1,8-diazabicyclo[5.4.0]undec-7-ene.
[b] DABCO = 1,4-Diazabicyclo[2.2.2]octane.
[c] TEA = Triethylamine.

targets and the compounds are showed in the Table 6. It is evident that the synthesized compounds have higher binding affinities than the standard antibiotics. Among the antibiotics, Ciprofloxacin showed the most potent binding affinity against all bacterial targets. On the other hand, Nystatin and Isoniazid showed the potent binding affinity against all fungal targets and *M.tb.* targets, respectively. Therefore, these standard compounds are used to compare the potency of the synthesized compounds. The binding interactions of compounds against the bacterial targets are shown in Figs. 1A and 1B; against the fungal targets are

shown in Figs. 2A and 2B; and against the *M.tb.* targets are depicated in Fig. 3 respectively.

Regarding the antibacterial activity, 1-Naphthol showed significant binding affinities than the standard antibacterial agents such as Norfloxacin, Chloramphenicol, and Ciprofloxacin towards all the crucial targets of the pathogenic bacteria as shown in the Table 4, Table 6, Fig. 1A, and Fig. 1B. Notably, 1-Naphthol showed −12 Kcal/mol, −12.5 Kcal/mol, −10.6 Kcal/mol against the Multidrug efflux pump submit AcrB of *E. coli,* TriABC of *P. aeruginosa,* and Multidrug Efflux Pump MepR of *S. aureus* respectively. 1-Naphthol showed a strong binding affinity with different bonds such as H-bonds and other hydrophobic interactions, and it possessed at least 1 H-bond with all the bacterial target proteins except the MexABOprM of *P. aeruginosa*, and Multidrug Efflux Pump MepR Cadmium efflux system accessory protein of *S. aureus*. Regarding the antifungal activity, all the 3 hit compounds namely 1-Naphthol **(7b)**, 2-Naphthol **(7c)**, and 3-Nitrophenol **(7e)** showed significant binding affinities than the standard antifungal agents such as Nystatin and Griseofulvin towards all the crucial targets of the pathogenic fungal as shown in the Table 5, Table 6, Figs. 2A, and Fig. 2B. Compounds **7b**, **7c** and **7e** showed significant binding affinities towards both the targets of *C. albicans,* and *A. niger* respectively. Notably, 3-Nitrophenol displayed binding energy of −12.5 Kcal/mol and −11.1 Kcal/mol against the Chitinase B and Prolyl endoprotease *A. niger* respectively. Similar to antifungal activity, all 3 hit compounds namely **7b**, **7c** and **7e** exhibited significant binding affinities than the standard antitubercular agent Isoniazid towards all the targets of crucial targets as shown in the Table 5, Table 6, and Fig. 3. 1-Naphthol, 2-Naphthol, and 3-Nitrophenol possessed −12 Kcal/mol, −12.5 Kcal/mol, and −11.7 Kcal/mol towards Enoyl-[acyl-carrier-protein] reductase, and −11.4 Kcal/mol, 12.1 Kcal/mol, and −11.4 Kcal/mol towards Topoisomerase I of *M.tb.* respectively. In contrast, 1-Naphthol, and 2-Naphthol couldn't make H-bond with the Topoisomerase I of *M.tb.* It is evident from the molecular docking study that compounds **7b**, **7c** and **7e** have significant binding affinities towards their respective protein targets in microorganisms due to their SAR activity [30].
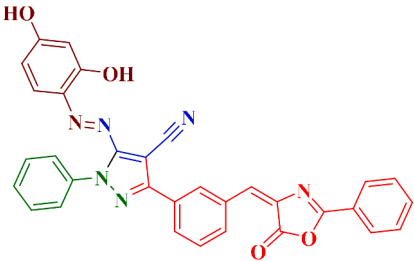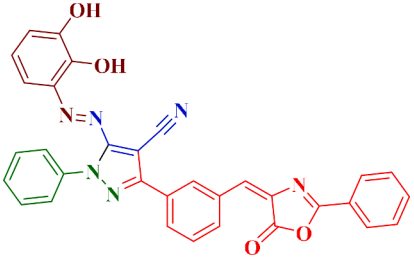
Anticancer evaluation
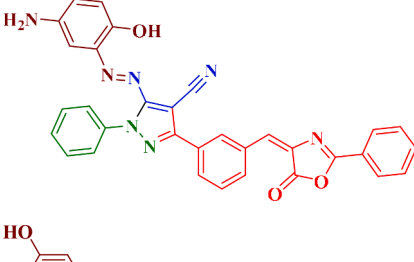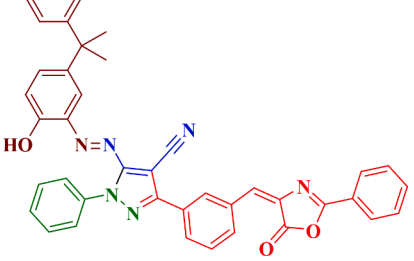
All ten synthesized compounds **(7a–j)** were tested for their

Table 2
Antimicrobial screening of the synthesized compounds **7a–j.**

Sr. No.	Ar—OH	Minimum inhibitory concentrations						
		For bacteria (MIC) in µg/mL				For fungi (MIC) in µg/mL		
		Gram-negative		Gram-positive		Fungi		
		E.C.[a]	*P.A.*[b]	*S.A.*[c]	*S.P.*[d]	*C.A.*[e]	*A.N.*[f]	*A.C.*[g]
7a		500	250	500	500	500	>1000	>1000
7b		25	100	50	50	100	250	500
7c		250	50	250	250	250	500	50
7d		500	500	100	100	500	500	250
7e		100	62.5	250	100	1000	100	1000
7f		250	250	500	500	500	1000	>1000

Table 2 (*continued*)

Sr. No.	Ar—OH	Minimum inhibitory concentrations						
		For bacteria (MIC) in µg/mL				For fungi (MIC) in µg/mL		
		Gram-negative		Gram-positive		Fungi		
		E.C.[a]	P.A.[b]	S.A.[c]	S.P.[d]	C.A.[e]	A.N.[f]	A.C.[g]
7g		500	>1000	N.E.[h]	500	>1000	100	N.E.
7h		>1000	500	250	500	N.E.	1000	1000
7i		500	1000	500	250	1000	>1000	500
7j		1000	500	500	500	>1000	N.E.	>1000
S.d.[i] 1	Chloramphenicol	50	50	50	50	–	–	–
S.d. 2	Ciprofloxacin	25	25	50	50	–	–	–
S.d. 3	Norfloxacin	10	10	10	10			
S.d. 4	Nystatin	–	–	–	–	100	100	100
S.d. 5	Griseofulvin	–	–	–	–	500	100	100

[a] *E.C.: Escherichia coli* MTCC 443.
[b] *P.A.:Pseudomonas aeruginosa* MTCC 1688.
[c] *S.A.: Staphylococcus aureus* MTCC 96.
[d] *S.P.: Staphylococcus pyogenes* MTCC 442.
[e] *C.A.: Candida albicans* MTCC 227.
[f] *A.N.: Aspergillus niger* MTCC 282.
[g] *A.C.: Aspergillus clavatus* MTCC 1323.
[h] N.E.: Non effective.
[i] S.d.: Standard drug.

effectiveness against cancer at a concentration of 10^{-5} M in the National Cancer Institute (NCI) in the USA, as part of the NCI's drug discovery program. They were tested using a one and five-dose anti-cancer assay, and the percentage of growth of treated cells is shown in Table 7. The results of the in-vitro anticancer primary screening studies showed that compound **7b** (NSC: D-849255/1) was the most effective against most cancer types, except for leukemia, with a mean growth percentage of −27.66 against various cancer cell lines. Additionally, compound **7a** (NSC: D-849254/1) showed good activity against leukemia, colon cancer, central nervous system cancer, melanoma, ovarian cancer, renal

Table 3

In vitro antitubercular screening data of analogues **7a–j**.

Sr. No.	% Inhibition (at 6.25 µg/mL)	MIC[a] µg/mL	IC$_{50}$[b] VERO cells	SI[c] (SI = IC$_{50}$/MIC)
7a	60	n.d.[d]	n.d.	n.d.
7b	94	0.06	>10	166.66
7c	89	1.56	8.5	5.448
7d	74	n.d.	n.d.	n.d.
7e	88	6.25	7.0	1.12
7f	79	n.d.	n.d.	n.d.
7g	67	n.d.	n.d.	n.d.
7h	62	n.d.	n.d.	n.d.
7i	73	n.d.	n.d.	n.d.
7j	70	n.d.	n.d.	n.d.
Isoniazid	99	0.03	>10	333.33

[a] Minimum inhibitory concentration against H$_{37}$Rv strain of *M. tuberculosis* (µg/mL).

[b] Measurement of cytotoxicity in VERO cells: 50% inhibitory concentrations (µg/mL).

[c] Selectivity index (*in vitro*): IC$_{50}$ in VERO cells/MIC against *M. tuberculosis*.

[d] n.d.: Not determined.

Table 4

Binding energies of compounds against the bacterial targets.

Organism	Target	Compound	Binding Energy (Kcal/mol)
Escherichia coli	CusC	Norfloxacin	−6.3
		Chloramphenicol	−6
		Ciprofloxacin	−6.7
		1-Naphthol	−9.7
	Multidrug efflux pump submit AcrB	Norfloxacin	−7.3
		Chloramphenicol	−6.7
		Ciprofloxacin	−8.3
		1-Naphthol	−12
Pseudomonas aeruginosa	MexABOprM	Norfloxacin	−5.9
		Chloramphenicol	−5.6
		Ciprofloxacin	−6.1
		1-Naphthol	−9.4
	TriABC	Norfloxacin	−7.3
		Chloramphenicol	−6.9
		Ciprofloxacin	−8.3
		1-Naphthol	−12.5
Staphylococcus aureus	Cadmium efflux system accessory protein	Norfloxacin	−6
		Chloramphenicol	−4.9
		Ciprofloxacin	−5.9
		1-Naphthol	−9.1
	Multidrug Efflux Pump MepR	Norfloxacin	−6.2
		Chloramphenicol	−5.8
		Ciprofloxacin	−6.1
		1-Naphthol	−10.6
Staphylococcus pyogenes	Tagatose-1,6-bisphosphate aldolase	Norfloxacin	−7.7
		Chloramphenicol	−7.3
		Ciprofloxacin	−7.9
		1-Naphthol	−9.9
	Streptopain	Norfloxacin	−5.6
		Chloramphenicol	−5.7
		Ciprofloxacin	−6.4
		1-Naphthol	−9.7

Table 5

Binding energies of compounds against the fungal and *M.tb.* targets.

Organism	Target	Compound	Binding Energy (Kcal/mol)
Candida albicans	Serine/Threonine phosphatase Z1	Nystatin	−7.4
		Griseofulvin	−6.7
		1-Naphthol	−9.3
	Sterol 14-alpha demethylase	Nystatin	−8.4
		Griseofulvin	−7.4
		1-Naphthol	−9.9
Aspergillus niger	Chitinase B	Nystatin	−10
		Griseofulvin	−7.4
		3-Nitrophenol	−12.5
	Prolyl endoprotease	Nystatin	−9.9
		Griseofulvin	−7.2
		3-Nitrophenol	−11.1
Aspergillus clavatus	Spherulin-4	Nystatin	−8.8
		Griseofulvin	−5.8
		2-Naphthol	−9.9
	M36 protease	Nystatin	−9.2
		Griseofulvin	−6.8
		2-Naphthol	−9.1
Mycobacterium tuberculosis	Enoyl-[acyl-carrier-protein] reductase	Isoniazid	−5.6
		1-Naphthol	−12
		3-Nitrophenol	−11.7
		2-Naphthol	−12.5
	Topoisomerase I	Isoniazid	−5.1
		1-Naphthol	−11.4
		3-Nitrophenol	−11.5
		2-Naphthol	−12.1

dose range, as they had demonstrated significant cell growth inhibition at a concentration of 10^{-5} M against various cancerous cell lines. Three response parameters were calculated for each cell line as an endpoint: (1) median growth inhibition (GI$_{50}$), (2) total growth inhibition (TGI) (cytostatic activity), and (3) median lethal growth inhibition (LC$_{50}$) (cytotoxic activity).

The GI$_{50}$, TGI, and LC$_{50}$ (in µM) values against subpanel cell lines are displayed in Table 8, indicating that **7b** (NSC: D-849255/1) displays high anticancer activity against all the breast cancer cell lines with GI$_{50}$ values ranging from 1.57 to 2.00 µM. This compound also demonstrated higher cytotoxic activity against BT-549 and MCF7 cell lines with TGI values 3.20 (LC$_{50}$ = 6.51 µM) and 3.56 µM (LC$_{50}$ = 7.79 µM), respectively. Additionally, Compound **7b** demonstrates good activity against PC-3 and DU-145 cell lines of prostate cancer, with GI$_{50}$ values of 1.34 and 1.83 µM and TGI values of 9.30 and 3.28 µM, respectively. The compound **7b** has demonstrated significant activity against renal cell lines. Its GI$_{50}$ values range from 1.26 to 1.99 µM against UO-31 cells (GI$_{50}$ = 1.26 µM), SN12C cells (GI$_{50}$ = 1.31 µM), RXF 393 cells (GI$_{50}$ = 1.36 µM), ACHN cells (GI$_{50}$ = 1.61 µM), and CAKI-1 cells (GI$_{50}$ = 1.99 µM). It has also exhibited notable TGI values against these five renal cancer cell lines, ranging from 2.66 to 7.56 µM. Excellent cytotoxicity was recorded against ovarian cancer with GI$_{50}$ values ranging from 1.40 µM to 2.97 µM against most of the tested cancer cell lines. Moreover, important TGI values ranging from 2.86 to 10.2 µM were detected against ovarian cell lines. This analogue confirmed notable anticancer activity against the entire panel of melanoma cancer cell lines with GI$_{50}$ values ranging from 1.44 to 2.23 µM. Its TGI values ranged from 2.78 to 5.35 µM, while lethality values (LC$_{50}$) ranged from 5.36 to 18.1 µM against all tested cancer cell lines. Moderate cytotoxicity was recorded against CNS cancer cells, except for SNB-75 cell line with a GI$_{50}$ value of 1.40 µM, and SF-539 cell line with a GI$_{50}$ value of 1.79 µM. Moreover,

cancer, and breast cancer, with a mean growth percentage of 25.07. The mean graph plots of growth percentage values for single doses are included in the supplementary material (Figs. S43–S52). Additionally, the anticancer analysis data for five doses, along with graphs of selected compounds **7a** and **7b**, can be found in the supplementary material (Figs. S53–S62).

After being selected, the same compounds were screened for a 5-log

Table 6

Interacting residues of the protein ligand complexes.

Complex	H-Bonds	Other interactions
CusC-Chloramphenicol	ASN133, GLU268, ASN279	ALA136, ALA272, ALA275, ALA276, ALA338, ARG341, GLN342, GLN344, SER345
CusC-1-Naphthol	GLN385	GLN160, ALA164, GLN167, ILE168, GLU171, THR172, ASN175, TYR176, GLN239, THR240, VAL241, GLN378, LEU381, LEU388, ARG392, GLU409, LEU412, PHE413, ARG416, LEU419, LEU420
Multidrug efflux pump submit AcrB-Chloramphenicol	GLN569	ALA33, GLN34, TYR35, THR37, ILE38, LEU293, ALA297, ASN298, ALA299, THR329, PHE332, VAL333, LEU668, PRO669, ALA670, ILE671, VAL672, GLU673
Multidrug efflux pump submit AcrB-1-Naphthol	PRO50, ASP53	TYR49, GLY51, ALA52, THR56, GLU121, GLN726, PHE727, LYS728, ILE729, LEU750, GLY751, TRP754, GLY756, SER757, TYR758, PRO783, ILE786, TRP809
MexABOprM-Chloramphenicol	–	PHE296, PHE297, PRO298, PRO333, ILE334, THR336, LEU340, ARG341
MexABOprM-1-Naphthol	–	THR178, THR181, TYR185, TYR185, THR219, TYR223, LEU389, ALA392, SER393, TYR396, ASP416, ARG419, SER420, THR423, ALA424, GLN426
TriABC-Chloramphenicol	LYS48, THR49, GLY845	PHE45, ILE47, TYR84, LYS86, TYR99, LEU100, ASP102, LEU608, PRO660, VAL661, GLY662, GLN666, ARG668, GLU849, GLU850, LYS853
TriABC-1-Naphthol	LEU812, ARG813	PHE549, PHE550, ARG638, LEU641, ARG642, TYR651, VAL652, GLU656, VAL661, ARG663, PRO664, GLY695, ASP696, SER811, ILE816, GLN817, PRO818, THR847
Cadmium efflux system accessory protein-Chloramphenicol	GLY84, HIS103	VAL32, ILE35, LEU36, GLN83, VAL85, GLN100, ASP101, ILE104, ILE107
Cadmium efflux system accessory protein-1-Naphthol	–	LEU36, ALA40, GLU42, ALA45, LYS46, TYR49, ILE107, MET108, ILE110, ALA111, LEU112
Multidrug Efflux Pump MepR-Chloramphenicol	THR49, GLN50, LYS89	ASN51, ARG79, ASP85, ARG87, ARG88
Multidrug Efflux Pump MepR-1-Naphthol	LEU57	GLU32, HIS35, GLY38, TYR39, TYR41, ALA42, ARG59, THR63, VAL64, LEU67, VAL101, PHE104, THR105, PHE108, GLU112
Tagatose-1,6-bisphosphate aldolase-Chloramphenicol	ARG29, GLU92, THR94	ASP27, GLN28, GLY30, ALA31, ARG34, ALA90, GLY95, LYS125, LEU127, TYR129, GLU163, LEU165, ASN174, LEU248, ARG278
Tagatose-1,6-bisphosphate aldolase-1-Naphthol	THR3, ASP202	LEU4, THR5, LYS8, MET12, GLY150, SER151, ARG154, GLU197, ARG198, GLY200, ASP242, LEU243, PRO244, MET326
Streptopain-Chloramphenicol	GLU174, LYS229, PHE232	LEU169, THR170, PRO171, VAL172, HIS187, PHE225, LEU231, ALA233, ALA234, ARG238, ALA266, ASP267, ILE270
Streptopain-1-Naphthol	GLN162, SER280, SER282, GLY339	ASN161, GLY191, CYS192, SER279, GLY281, ALA283,

Table 6 (*continued*)

Complex	H-Bonds	Other interactions
		GLN332, VAL334, VAL337, GLY338, HIS340, TRP359, VAL362, ALA376, LEU377, PHE386
Serine/Threonine phosphatase Z1-Nystatin	GLU219, ARG352, ARG356	LEU212, SER213, GLN214, PRO215, SER216, LEU217, LEU218, LEU220, ALA355
Serine/Threonine phosphatase Z1-1-Naphthol	PRO343	LEU341, SER342, LEU345, GLU380, TRP381, GLU382, ASP383, TYR390, ALA396, LYS399, PHE400, SER402, LYS403
Sterol 14-alpha demethylase-Nystatin	GLU194, SER222	THR172, GLU174, LYS177, LYS190, ILE197, PHE198, PHE213, ARG215, ALA218, TYR221, ASP225, GLN309
Sterol 14-alpha demethylase-1-Naphthol	HIS377	PHE58, ALA61, TYR64, GLY65, LEU87, LEU88, PRO230, ILE231, PHE233, VAL234, PHE235, LEU376, SER378, PHE380, TYR505, SER506, MET508
Chitinase B-Nystatin	TRP109, GLU149, TYR150, LYS196, MET215, GLU294	TRP25, TYR111, SER191, ALA192, GLY193, TYR217, ASP218, TRP223, ARG273, TRP356
Chitinase B-3-Nitrophenol	ARG30, ARG273, ASP299, GLU357	PHE49, TRP109, TYR150, ALA192, GLY193, MET215, TYR217, ASP218, TYR219, TRP223, PHE245, TYR271, TRP293, GLU294, VAL297, TRP356
Prolyl endoprotease-Nystatin	TYR496	VAL89, TYR94, ASP267, ALA270, VAL271, ASN274, TYR277, GLN280, ASP281, TYR335, TYR339, CYS350, PHE351, ILE360, PRO369, VAL370, ASP371, TYR406, TRP407, TYR414, HIS491, CYS492
Prolyl endoprotease-3-Nitrophenol	ASP267, CYS350, PHE351, GLN387, TYR406	PRO86, GLU88, VAL89, TYR94, SER179, TYR215, ALA270, ASN274, TYR277, GLN280, TYR335, ASP352, SER353, GLU375, LEU378, TRP386, TRP407, GLN410, TRP460
Spherulin-4-Nystatin	ASN93, SER96, GLU167, TYR287	TYR65, PRO94, GLY95, TYR126, ALA128, ASP166, GLU222, ALA223, THR224, THR227, HIS253, TYR288
Spherulin-4—2-Naphthol	PRO203, HIS253	GLU32, HIS35, GLY38, TYR39, TYR41, ALA42, ARG59, THR63, VAL64, LEU67, VAL101, PHE104, THR105, PHE108, GLU112
M36 protease-Nystatin	ASN147, ASN149, ARG160, GLU185, HIS275	ALA148, PHE150, ALA151, THR152, PRO153, PRO154, ARG162, TYR164, HIS184, HIS188, GLU214
M36 protease-2-Naphthol	THR152, ASN192	PHE150, ALA151, PRO153, PRO154, GLN157, HIS188, SER201, ASN202, LEU204, SER205, ILE207, GLY210, GLY213, ASP272, VAL274
Enoyl-[acyl-carrier-protein] reductase-Isoniazid	SER143, SER147	ASN77, LEU81, LEU95, PHE116, TYR123, LEU124, LYS146
Enoyl-[acyl-carrier-protein] reductase-1-Naphthol	SER147	THR70, ILE73, ASN77, THR80, LEU81, TYR84, TRP97, GLU114, PHE116, TYR123, LEU124, TRP133, SER143, LYS146, GLU152, HIS155, GLN156, ALA158, TYR159, THR163

Table 6 (*continued*)

Complex	H-Bonds	Other interactions
Enoyl-[acyl-carrier-protein] reductase-2-Naphthol	THR70	TYR7, HIS9, MET45, TYR59, ARG62, GLU63, SER66, ALA67, ASP69, ILE73, PHE74, ASN77, TRP97, HIS99, PHE116, LEU124, TRP133, SER147, GLU152, TYR159, THR163, TRP167, TYR171
Enoyl-[acyl-carrier-protein] reductase-3-Nitrophenol	TYR159	LEU5, TYR7, HIS9, TYR59, GLU63, SER66, ALA67, ASP69, THR70, ILE73, PHE74, ASN77, TRP97, HIS99, PHE116, LEU124, SER143, SER147, GLU152, HIS155, GLN156, THR163, CYS164, TRP167, TYR171
Topoisomerase I-Isoniazid	VAL195, GLN196	ASP171, GLY193, ARG194, SER197, SER539, ILE540, THR543
Topoisomerase I-1-Naphthol	–	GLU24, SER25, PRO26, ARG46, GLY47, HIS48, ASP113, GLU115, ILE119, ARG167, ARG194, VAL195, GLN196, TYR342, ARG344, HIS389, GLY532, ARG533, SER535, THR536, SER539, ILE540, THR543
Topoisomerase I-2-Naphthol	–	GLU24, SER25, ARG46, GLY47, HIS48, ASP113, GLU115, ILE119, ARG167, ARG194, VAL195, GLN196, TYR342, ARG344, HIS389, GLY532, ARG533, PRO534, SER535, THR536, SER539, ILE540, THR543
Topoisomerase I-3-Nitrophenol	GLU24, GLY47	GLU24, SER25, PRO26, ARG46, HIS48, ASP113, GLU115, ARG167, ARG194, VAL195, GLN196, TYR342, ARG344, HIS389, GLY532, ARG533, PRO534, SER535, THR536, SER539, ILE540, THR543

good TGI values ranging from 2.78 to 17.4 μM were obtained against CNS cancerous cell lines. This compound demonstrated moderate anticancer activity against colon and lung cancer cell lines, with GI_{50} values ranging from 1.43 to 16.4 μM. However, slightly higher cytostatic values ranging from 3.15 to 30.3 μM were observed, along with higher range lethality values of 5.99 to more than 100 μM. Furthermore, compound **7b** was tested for anticancer activity against a panel of leukemic cancer cell lines. The results showed that the compound had weak activity, with GI_{50} values ranging from 2.02 to 3.41 μM. It only showed a TGI value of 7.97 μM for the CCRF-CEM cell line, while for lethality (LC_{50} values), it had values exceeding 100 μM toward all selected panel cancer cell lines [31].

On the other hand, compound **7a** (NSC: D-849254/1) exhibited remarkable anticancer activity against the colon, melanoma, ovarian, renal and breast cancer cell lines with GI_{50} values ranging from 1.60 to 2.55 μM. Accepted pronounced TGI as well as LC_{50} values were recorded against HCT-116 colon (TGI = 3.87 & LC_{50} = 8.11 μM), LOX IMVI melanoma (TGI = 8.39 & LC_{50} = 35.9 μM), OVCAR-3 ovarian (TGI = 4.03 & LC_{50} = 8.50 μM), ACHN renal (TGI = 5.63 & LC_{50} = 20.7 μM), UO-31 renal (TGI = 6.45 & LC_{50} = 26.8 μM), and MDA-MB-468 breast (TGI = 3.62 & LC_{50} = 8.23 μM) cancer cell lines. All the five-dose response curves of **7a** and **7b** against the full panel of 60 human cancer cell lines are presented in Figs. 4, 5 and Table 8 which include nine tumor subpanels cancer cell lines [32].

SAR study

Substituents with a phenol group on fused rings were found to significantly increase antimicrobial, antitubercular and anticancer activity. **Antimicrobial SAR:** In comparison to other substituted phenolic rings in the periphery, the benzo-fused phenol ring (1-Naphthol) demonstrated excellent antimicrobial activity against selected gram-negative bacteria, while 2-Naphthol enhanced the antifungal activity against *Aspergillus clavatus* strain. The results also prove that the compound with an EWG (—NO_2) attached at the *meta* position of the substituted ring system indicated a moderate increase in antimicrobial activity. Furthermore, the substitution of EDGs at any position on the phenolic ring system was found to be responsible for the reduction of antimicrobial activity [33]. **Antitubercular SAR:** It has been found that 1-Naphthol has potential as an antitubercular agent, with the highest percentage inhibition and selectivity index against *M. tuberculosis*. On the other hand, 2-Naphthol exhibited good percentage inhibition but may be less potent in IC_{50} in VERO cell lines. It has also been discovered that compounds with electron-withdrawing groups (EWGs) and electron-donating groups (EDGs) in any substituted positions on the phenol ring were responsible for the weak antitubercular activity [34]. **Anticancer SAR:** It has been observed that a type of benzo-fused phenol called 1-Naphthol, **7b**, has significantly higher anticancer activity against all types of cancer compared to other phenol derivatives. This compound has shown good growth percentage on active cancer cell lines. Similarly, a simple phenol compound **7a** has displayed good anticancer activity against selected types of cancer such as Leukemia, Colon, Central Nervous, Melanoma, Ovarian, Renal, and Breast cancer cell lines. However, the addition of other electron-donating groups (EDGs) and electron-withdrawing groups (EWGs) substitutions on various positions of the core nucleus have led to a decrease in the cancer activity of these compounds (Fig. 6) [35].

Conclusion

The objective of this study was to create new pyrazole derivatives containing oxazolone using various basic catalysts for the treatment of infectious and fetal diseases. The best catalyst was found to be DBU, which produced excellent yields when using ethanol and water as solvents. Compound **7b**, which contains 1-Naphthol, was effective against *E. coli* (25 μg/mL), *S. aureus* (50 μg/mL), and *S. pyogenes* (50 μg/mL). Compound **7c** (2-Naphthol) was effective against *P. aeruginosa* (50 μg/mL) and *A. clavatus* (50 μg/mL) strains, similar to standard drugs. Notably, the compounds with benzo-fused phenol groups (**7b** and **7c**) and EWG (—NO_2) in the *meta* position (**7e**) demonstrated higher antimicrobial activity than the ones with substituted groups in the *ortho* and *para* positions. Compound **7b** was the most potent in the antitubercular study, with 94 % inhibition and 0.06 μg/mL against *M. tuberculosis* H37Rv strain. In a computational study, compounds **7b** and **7e** showed significant binding affinity (−12.5 to −9.1 Kcal/mol) with interacting residues against various bacterial and fungal targets. Additionally, similar molecules (**7b**, **7c** and **7e**) exhibited proficient binding affinity against Enoyl-[acyl-carrier-protein] reductase and Topoisomerase I targets of *M. tuberculosis*. Compound **7b** has been found to have excellent cytotoxic activity against all types of cancer, except leukemia. It has good GI_{50} values, ranging from 1.26 to 1.83 μM, and LC_{50} values ranging from 5.36 to 7.88 μM. On the other hand, compound **7a** has remarkable antitumor potency against colon, melanoma, ovarian, renal, and breast cancer cell lines, with growth inhibitory activity (GI_{50}) values ranging from 1.60 to 2.55 μM. Taken together, **7b** could be a valuable lead molecule for treating microbial infections, tuberculosis, and cancer due to its favorable drug-like features.
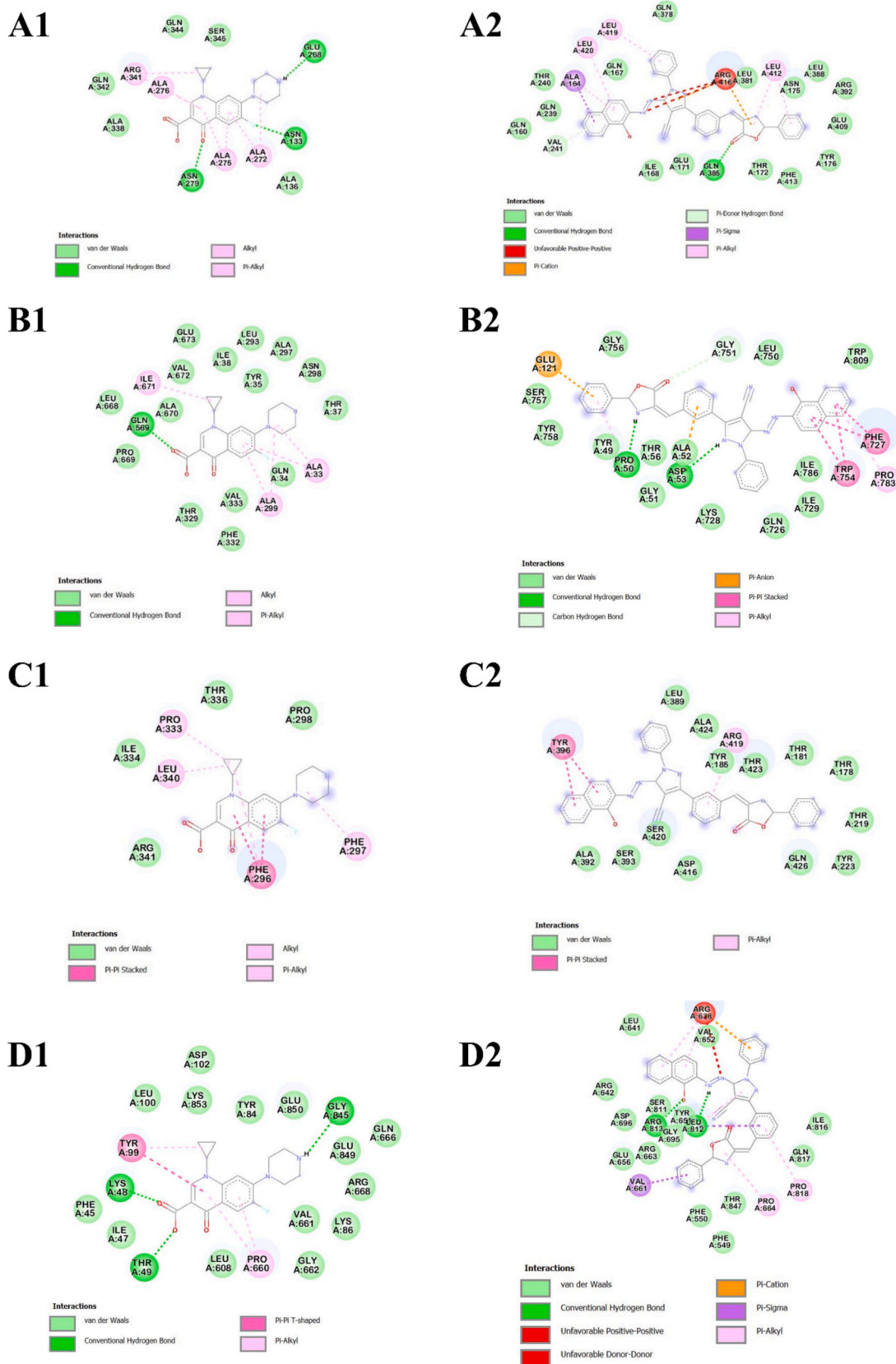
Fig. 1A. Binding interaction of compounds against bacterial targets: 2D interaction of Ciprofloxacin (A1–D1) and 1-Napthol (A2–D2) against the CusC, Multidrug efflux pump submit AcrB, MexABOprM, and TriABC are shown respectively.
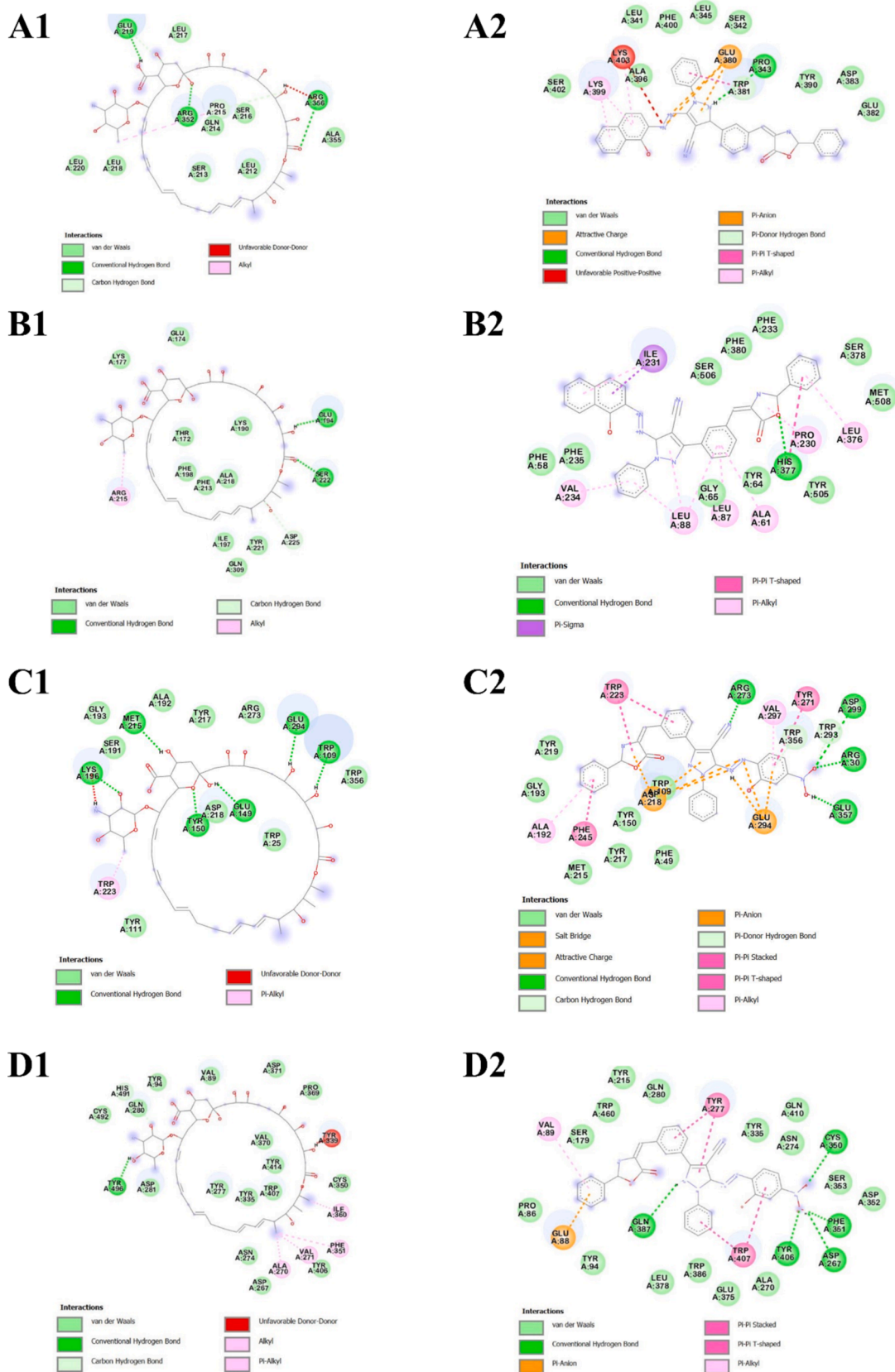
Fig. 1B. Binding interaction of compounds against bacterial targets: 2D interaction of Ciprofloxacin (E1–H1) and 1-Napthol (E2–H2) against the Cadmium efflux system accessory protein, Multidrug Efflux Pump MepR, Tagatose-1,6-bisphosphate aldolase, and Streptopain are shown respectively.

Fig. 2A. Binding interaction of compounds against fungal targets: 2D interaction of Nystatin (A1–B1) and 1-Napthol (A2–B2) against Serine/Threonine phosphatase Z1, and Sterol 14-alpha demethylase; Nystatin (C1–D1) and 3-Nitrophenol (C2–D2) are shown respectively.
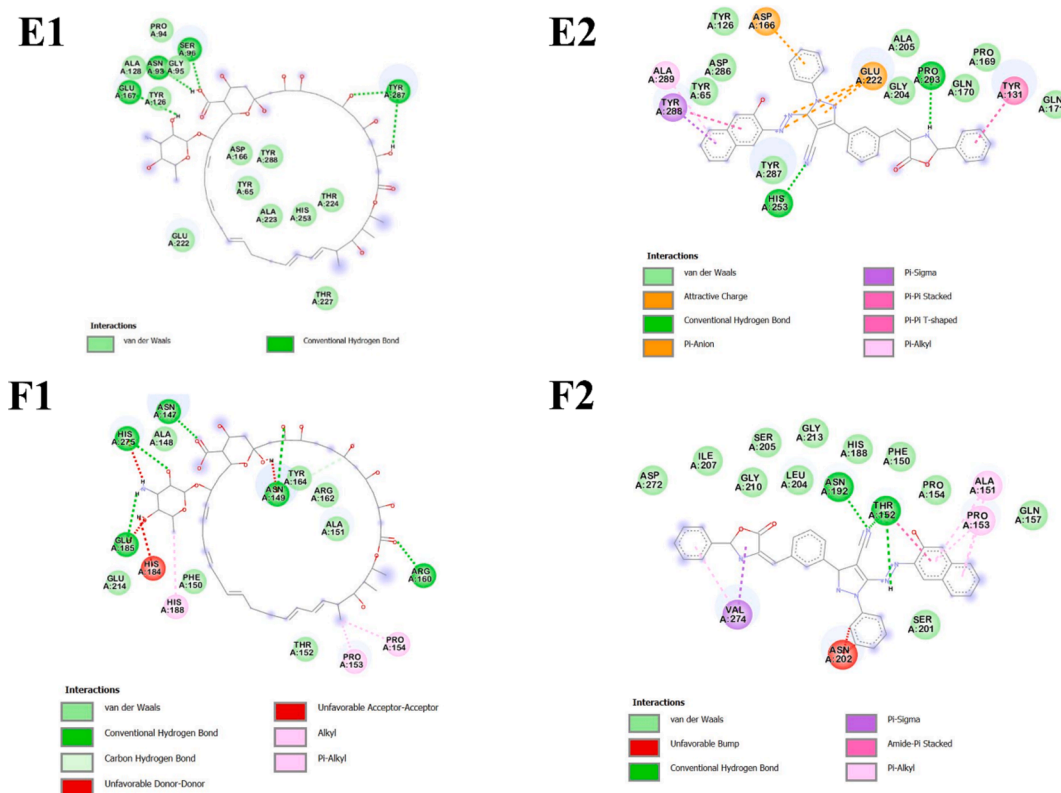
Fig. 2B. Binding interaction of compounds against fungal targets: 2D interaction of Nystatin (E1–F1) and 2-Napthol (E2–F2) against Chitinase B, and Prolyl endoprotease are shown respectively.

Experimental section

Materials and physical measurements

All chemicals were used as AnalaR grade for synthesis. The [1]H (400 and 500 MHz) and ^{13}C NMR (100 MHz) spectra were recorded on a Bruker ultra-shield spectrometer using DMSO-d_6 as the solvent and tetramethylsilane (TMS) as an internal standard for chemical shifts. Coupling constants (*J*) are expressed in hertz (Hz), and abbreviations such as s (singlet), d (doublet), t (triplet), and m (multiplet) are utilized. Mass spectra were recorded using a SHIMADZU GC-2010+ ultra LCMS spectrometer. Infrared spectra (ν, cm^{-1}) were obtained on a Shimadzu FTIR 8400S spectrophotometer. Elemental analyses were conducted with an ECS 4010 Elemental Combustion System (Costech Instruments, Pioltello), and the results fell within the accepted range (± 0.40) of the calculated values. Melting points were determined using an electrothermal melting point apparatus (model 9100, Electrothermal Engineering Ltd.), and the results are reported uncorrected. The completion of reactions was monitored on a 20×20 cm aluminum-coated TLC plate (60 F245, E. Merck) using a mobile phase of n-hexane and ethyl acetate (7:3). Visualization of the plates was performed under ultraviolet (UV) light or in an iodine chamber.

Synthesis of 3-((5-oxo-2-phenyloxazol-4(5H)-ylidene)methyl) benzaldehyde (3)

A mixture of isophthalaldehyde **(1)** (0.01 mol), hippuric acid (0.01 mol), acetic anhydride (0.01 mol) and anhydrous sodium acetate (0.01 mol) was taken in a round bottom flask and heated with constant stirring. As soon as the mixture completely liquefied, the flask was transferred to a water bath and further heated for 4 h. After the reflux, ethanol was added slowly to the flask and the mixture was allowed to stand overnight in refrigerator. The crystalline whitish product obtained

was filtered and washed with ice-cold alcohol [36]. ^{1}H NMR (400 MHz, DMSO-d_6): δ ppm 10.07 (s, 1H, CHO), 8.51–8.49 (d, *J* = 8.4 Hz, 1H, Ar—H), 8.45 (s, 1H, Ar—H), 8.19–8.17 (d, *J* = 7.2 Hz, 2H, Ar—H), 8.05–8.03 (d, *J* = 8.4 Hz, 2H, Ar—H), 7.78–7.74 (t, *J* = 7.2 Hz, 1H. Ar—H), 7.68–7.65 (t, *J* = 7.6 Hz, 2H, Ar—H), 7.43 (s, 1H, ═CH). LCMS: calcd. *m/z* 277.28, found *m/z* 276.9 [M$^+$].

Synthesis of 5-amino-3-(3-((5-oxo-2-phenyloxazol-4(5H)-ylidene) methyl)phenyl)-1-phenyl-1H-pyrazole-4-carbonitrile (6)

In a 50 ml round bottom flask, 20 ml of 50 % v/v ethanol and distilled water were combined. Malononitrile **(4)** was added to the solution, followed by the addition of DBU catalyst (0.1 mmol) to the ethanolic solution. The mixture was stirred on a magnetic stirrer. Next, 3-((5-oxo-2-phenyloxazol-4(5*H*)-ylidene)methyl)benzaldehyde **(3)** was introduced to the mixture, and stirring continued for about 2–3 min until the solution turned light yellow. Phenylhydrazine **(5)** was added to this solution, and after stirring, an orange color appeared in the reaction mixture. The stirring process continued for 100 min at room temperature until the reaction was complete. The reaction completion was monitored through TLC using n-hexane and ethyl acetate (7:3) solvent system. The product was filtered off, washed with water, dried, and purified through chromatography [37].

General procedure for synthesis of 5-(2-(aryl)diazenyl)-3-(3-(5-oxo-2-phenyloxazol-4(5H)-ylidene)methyl)phenyl)-1-phenyl-1H-pyrazole-4-carbonitrile (7a–j)

A solution of 5-amino-3-(3-((5-oxo-2-phenyloxazol-4(5*H*)-ylidene) methyl)phenyl)-1-phenyl-1*H*-pyrazole-4-carbonitrile **(6)** (0.01 mol) was prepared in minimum amount of HCl (2 ml). A cold solution of sodium nitrite below 5 °C was then added to it with continuous stirred. A solution of various phenol derivative (0.01 mol) was prepared by

Fig. 3. Binding interaction of compounds against *M.tb.* targets: 2D interaction of Isoniazid (A & E), 1-Napthol (B & F), 2-Napthol (C & G), 3-Nitrophenol (D & H) against Spherulin-4 and M36 protease are shown respectively.

Table 7
Growth and mean growth percentage data of subpanel of tumor cell lines at single-dose (10^{-5} M) concentration.

Entry	NCI code	Cancer Type	Active Cell Lines	Growth Percent	Mean Growth Percent
7a	NSC: D-849254/1	L	NSCLC	−50.64	25.07
		CC	HCT-116	−79.87	
			HCT-15	−7.80	
			SW-620	−50.46	
		CNSC	U251	−42.27	
		M	LOX IMVI	−53.91	
			MDA-MB-435	−56.42	
		OC	IGROV1	−19.71	
			OVCAR-3	−75.09	
			NCI/ADR-RES	−30.19	
		RC	786–0	−12.60	
			ACHN	−98.58	
			RXF 393	−7.84	
			SN12C	−19.53	
		BC	MCF7	−62.61	
			T-47D	−58.40	
			MDA-MB-468	−33.07	
7b	NSC: D-849255/1	NSCLC	EKVX	−54.76	−27.66
			HOP-62	−71.70	
			NCI-H226	−66.05	
			NCI-H23	−44.65	
			NCI-H522	−73.09	
		CC	COLO 205	−77.60	
			HCT-116	−30.79	
			HCT-15	−23.17	
			SW-620	−24.87	
		CNSC	SF-539	−88.29	
			SNB-19	−0.45	
			SNB-75	−92.88	
			U251	−45.04	
		M	LOX IMVI-51.74	−51.74	
			MALME-3M	81.73	
			M14	−63.99	
			MDA-MB-435	65.47	
			SK-MEL-2	−53.64	
			SK-MEL-28	−80.62	
			SK-MEL-5	−96.71	
			UACC-257	−87.61	
			UACC-62	−78.67	
		OC	IGROV1	−12.56	
			OVCAR-3	−21.78	
			OVCAR-4	−86.94	
			OVCAR-5	−90.82	
			SK-OV-3	−83.21	
		RC	786–0	−31.37	
			ACHN	−99.91	
			RXF 393	−44.07	
			SN12C	−95.80	
			UO-31	−42.27	
		PC	PC-3	−24.30	
			DU-145	−85.33	
		BC	MCF7	−64.07	
			MDA-MB-231/ATCC	−10.44	
			HS 578 T	−1.24	
			BT-549	−86.17	
			T-47D	−45.84	
			MDA-MB-468	−38.92	
7c	NSC: D-849256/1	M	MDA-MB-435	−66.20	70.39
		OC	OVCAR-3	−2.11	

Table 7 (*continued*)

Entry	NCI code	Cancer Type	Active Cell Lines	Growth Percent	Mean Growth Percent
7d	NSC: D-849257/1	M	UACC-62	57.33	87.87
7e	NSC: D-849258/1	M	SK-MEL-5	17.72	88.63
7f	NSC: D-849259/1	CC	COLO 205	77.65	102.23
7g	NSC: D-849260/1	NSCLC	NCI-H522	−69.63	82.16
		CC	HCT-15	−17.05	
7h	NSC: D-849261/1	M	SK-MEL-5	68.18	98.38
7i	NSC: D-849262/1	M	SK-MEL-5	73.89	105.39
7j	NSC: D-849263/1	L	MOLT-4	51.66	86.08

L: Leukemia; NSCLC: Non-Small Cell Lung Cancer; CC: Colon Cancer; CNSC: Central Nervous System Cancer; PC: Prostate Cancer; OC: Ovarian Cancer; RC: Renal Cancer; BC: Breast Cancer; M: Melanoma.

dissolving in sodium hydroxide solution then cooled to 0 °C. The cold diazonium salt was added to solution of phenol derivative in sodium hydroxide kept at 0 °C. The solid dye was filtered out, dried and recrystallized from ethanol [38].

*5-(-(2-hydroxyphenyl)diazenyl)-3-(3-(-(5-oxo-2-phenyloxazol-4(5H)-ylidene)methyl)phenyl)-1-phenyl-1H-pyrazole-4-carbonitrile (**7a**)*

Yield: 92 %. m.p. 300–302 °C. FTIR (KBr, cm^{-1}): 1250 (s, C—N), 1637 (s, C=O), 2195 (s, CN), 2972 (w, C—H), 3319 (b, O—H). ^{1}H NMR (500 MHz, DMSO-d_6): δ ppm 9.72 (s, 1H, OH), 7.82–7.80 (d, J = 7.8, 1.5 Hz, 4H, =CH & Ar—H), 7.76 (s, 1H, Ar—H), 7.58–7.52 (dd, J = 7.5, 1.5 Hz, 3H, Ar—H), 7.42–7.37 (m, 2H, Ar—H), 7.32–7.27 (m, 5H, Ar—H), 7.15–7.10 (dd, J = 7.5, 1.5 Hz, 2H, Ar—H), 6.90–6.83 (m, 2H, Phenolic Ar—H). ^{13}C NMR (100 MHz, DMSO-d_6): δ ppm 166.70 (Oxazolone-C—Ar), 162.01 (C=O), 161.89 (Pyrazole-C—N), 158.26 (C—OH), 138.89 (Pyrazole-C=N), 138.83 (Ar—C), 138.27 (Phenolic C), 135.84 (=CH), 133.99 (Ar—C), 132.94 (Ar—C), 132.35 (Ar—C), 132.03 (Ar—C), 130.28 (Ar—C), 129.37 (Ar—C), 129.16 (4)(Ar—C), 128.41 (Ar—C), 127.88 (2)(Ar—C), 126.23 (Oxazolone-C=C), 125.90 (Ar—C), 124.86 (3)(Ar—C), 123.39 (Ar—C), 122.36 (Phenolic-C), 121.15 (Phenolic-C), 117.10 (Phenolic-C), 116.55 (CN), 86.68 (C—CN). LCMS: calcd. m/z 536.16, found m/z 536 [M$^+$]. Anal. calc for: $C_{32}H_{20}N_6O_3$: C, 71.63; H, 3.76; N, 15.66; Found: C, 71.61; H, 3.78; N, 15.63 %.

*5-(-(1-hydroxynaphthalen-2-yl)diazenyl)-3-(3-(-(5-oxo-2-phenyloxazol-4(5H)-ylidene)methyl)phenyl)-1-phenyl-1H-pyrazole-4-carbonitrile (**7b**)*

Yield: 89 %; m.p. 78–80 °C; FTIR (KBr, cm^{-1}): 1261 (s, C—N), 1630 (s, C=O), 2202 (s, CN), 3057 (w, C—H), 3329 (b, O—H). ^{1}H NMR (500 MHz, DMSO-d_6): δ ppm 7.89–7.79 (d, J = 7.5, 1.5 Hz, 4H, =CH & Ar—H), 7.73 (s, 1H, Phenolic Ar—H), 7.60–7.57 (d, J = 7.5, 1.5 Hz, 5H, Ar—H), 7.41 (s, 1H, Ar—H), 7.38 (s, 1H, Ar—H), 7.30–7.28 (m, 6H, Ar—H), 7.23–7.21 (d, J = 7.5, 1.5 Hz, 2H, Phenolic Ar—H), 7.14–7.11 (t, J = 7.5, 1.5 Hz, 1H, Ar—H), 6.65 (s, 1H, OH). ^{13}C NMR (100 MHz, DMSO-d_6): δ ppm 166.70 (Oxazolone-C—Ar), 162.01 (C=O), 161.89 (Pyrazole-C—N), 151.25 (C—OH), 138.89 (Pyrazole-C=N), 138.83 (Ar—C), 135.84 (=CH), 135.20 (Phenolic-C), 133.99 (Ar—C), 132.94 (Ar—C), 132.03 (Ar—C), 130.65 (Phenolic-C), 130.28 (Ar—C), 129.37 (Ar—C), 129.16 (4)(Ar—C), 128.67 (Phenolic-C), 128.41 (Ar—C), 127.88 (2)(Ar—C), 127.59 (Phenolic-C), 127.18 (Phenolic-C), 126.37 (Phenolic-C), 126.24 (2)(Phenolic-C & Oxazolone-C=C), 125.90 (Ar—C), 125.80 (Phenolic-C), 124.86 (3)(Ar—C), 123.39 (Ar—C), 122.34 (Phenolic-C), 116.55 (CN), 86.68 (C—CN). LCMS: calcd. m/z 586.18, found m/z 587 [M$^+$]. Anal. calc for: $C_{36}H_{22}N_6O_3$: C, 73.71; H,

Table 8

GI$_{50}$, TGI, and LC$_{50}$ values (in μM) of anticancer activity data, as per five doses of compound **7a** and **7b**.

Cell line[a]	Compound					
	7a (NSC: D-849254/1)			**7b** (NSC: D-849255/1)		
	GI$_{50}$	TGI	LC$_{50}$	GI$_{50}$	TGI	LC$_{50}$
Leukemia						
CCRF-CEM	1.35	7.21	>100	2.39	7.97	>100
HL-60(TB)	2.99	>100	>100	2.02	>100	>100
K-562	2.77	>100	>100	3.41	>100	>100
MOLT-4	3.08	>100	>100	3.39	>100	>100
RPMI-8226	2.04	8.45	>100	2.23	–	>100
SR	2.44	>100	>100	2.69	>100	>100
Non-Small Cell Lung Cancer						
A549/ATCC	39.0	>100	>100	3.41	19.0	>100
EKVX	10.4	23.2	51.6	1.93	4.65	14.7
HOP-62	15.7	33.2	70.2	2.14	7.69	42.3
HOP-92	4.26	20.5	81.1	2.60	10.2	49.8
NCI-H226	16.9	36.2	77.6	2.15	7.58	>100
NCI-H23	11.8	29.1	71.8	1.43	3.36	7.88
NCI-H322M	13.5	26.8	53.3	10.4	22.5	48.5
NCI-H460	17.8	47.7	>100	3.76	19.0	>100
NCI-H522	3.28	11.1	42.1	**1.65**	**3.15**	**5.99**
Colon Cancer						
COLO 205	6.24	19.1	45.8	1.81	4.38	11.7
HCC-2998	18.0	32.3	58.0	16.4	30.3	56.0
HCT-116	**1.84**	**3.87**	**8.11**	1.78	5.73	30.6
HCT-15	4.17	19.6	81.3	**1.80**	**3.77**	**7.88**
HT29	4.36	16.7	64.9	1.73	4.72	>100
KM12	12.2	26.2	56.2	2.84	11.4	37.5
SW-620	1.87	4.17	–	1.76	4.09	–
CNS Cancer						
SF-268	14.5	32.6	73.2	2.97	10.7	37.7
SF-295	16.0	30.5	57.8	4.81	17.4	44.6
SF-539	7.89	21.9	51.6	1.79	3.30	6.09
SNB-19	14.8	28.4	54.5	2.23	6.17	23.1
SNB-75	10.3	22.8	50.4	**1.40**	**2.78**	**5.53**
U251	4.31	>100	>100	2.23	5.28	>100
Melanoma						
LOX IMVI	**2.55**	**8.39**	**35.9**	1.54	3.30	7.10
MALME-3M	10.0	24.3	59.0	**1.44**	**2.78**	**5.36**
M14	12.9	26.3	53.8	**1.58**	**2.98**	**5.62**
MDA-MB-435	7.72	21.8	53.3	1.88	3.47	6.41
SK-MEL-2	13.3	28.2	59.4	1.63	3.39	7.02
SK-MEL-28	10.1	22.9	52.3	2.23	5.35	18.1
SK-MEL-5	14.3	28.5	56.6	**1.63**	**3.00**	**5.54**
UACC-257	17.6	38.5	84.1	1.80	3.39	6.41
UACC-62	10.9	24.4	54.7	1.71	3.22	6.06
Ovarian Cancer						
IGROV1	5.31	19.7	52.4	1.41	3.17	7.09
OVCAR-3	**1.91**	**4.03**	**8.50**	1.40	3.71	9.84
OVCAR-4	6.06	18.9	44.2	**1.46**	**2.86**	**5.57**
OVCAR-5	9.61	22.4	50.9	1.76	3.65	7.55
OVCAR-8	3.16	11.7	52.2	2.97	10.2	52.5
NCI/ADR-RES	3.04	19.2	>100	2.34	7.20	53.6
SK-OV-3	15.5	32.8	69.4	7.25	22.4	53.0
Renal Cancer						
786-0	3.13	9.98	45.6	4.60	22.9	91.7
A498	19.2	34.1	60.5	15.8	29.6	55.3
ACHN	**1.99**	**5.63**	**20.7**	**1.61**	**3.34**	**6.96**
CAKI-1	4.52	18.3	46.5	1.99	7.56	29.6
RXF 393	14.7	28.2	54.1	1.36	3.97	13.4
SN12C	5.19	18.5	44.0	**1.31**	**2.66**	**5.37**
TK-10	19.3	33.6	58.4	15.1	28.6	54.2
UO-31	**1.70**	**6.45**	**26.8**	1.26	3.15	7.86

Table 8 (*continued*)

Cell line[a]	Compound					
	7a (NSC: D-849254/1)			**7b** (NSC: D-849255/1)		
	GI$_{50}$	TGI	LC$_{50}$	GI$_{50}$	TGI	LC$_{50}$
Prostate Cancer						
PC-3	6.26	27.2	94.6	1.34	9.30	49.7
DU-145	14.6	28.5	55.5	**1.83**	**3.28**	**5.88**
Breast Cancer						
MCF7	2.10	4.61	>100	1.63	3.56	7.79
MDA-MB-231/ATCC	3.06	12.1	43.3	2.00	6.75	29.6
HS 578T	15.3	62.2	>1.00	1.75	4.68	36.6
BT-549	4.90	20.0	49.1	**1.57**	**3.20**	**6.51**
T-47D	2.23	5.39	>1.00	1.75	4.66	>100
MDA-MB-468	**1.60**	**3.62**	**8.23**	1.96	5.11	34.0

The GI$_{50}$, TGI, and LC$_{50}$ values of the potent compound were written in bold and italics.

"–" means not tested.

  [a] Data derived from NCI-60 human cell lines.

3.78; N, 14.33; Found: C, 73.73; H, 3.80; N, 14.31 %.

5-(-(3-hydroxynaphthalen-2-yl)diazenyl)-3-(3-(-(5-oxo-2-phenyloxazol-4(5H)-ylidene)methyl)phenyl)-1-phenyl-1H-pyrazole-4-carbonitrile (7c)

Yield: 90 %. m.p. 98–100 °C. FTIR (KBr, cm^{-1}): 1236 (s, C—N), 1668 (s, C=O), 2177 (s, CN), 3045 (m, C—H), 3542 (b, O—H). ^{1}H NMR (500 MHz, DMSO-d_6): δ ppm 8.25 (d, J = 1.4 Hz, 1H, Phenolic Ar—H), 7.82–7.80 (m, 3H, =CH & Ar—H), 7.76 (t, J = 1.2 Hz, 1H, Ar—H), 7.63 (d, J = 7.5 Hz, 1H, Ar—H), 7.58–7.44 (m, 4H, Ar—H), 7.42–7.35 (m, 2H, Ar—H), 7.34–7.22 (m, 7H, Ar—H), 7.21 (d, J = 1.4 Hz, 1H, Phenolic Ar—H), 7.11 (s, 1H, Ar—H), 6.78 (d, J = 1.7 Hz, 1H, Phenolic Ar—H), 5.25 (s, 1H, OH). ^{13}C NMR (100 MHz, DMSO-d_6): δ ppm 166.70 (Oxazolone-C—Ar), 162.01 (C=O), 161.89 (Pyrazole-C—N), 156.47 (C—OH), 138.89 (Pyrazole-C=N), 138.83 (Ar—C), 135.84 (=CH), 134.13 (Phenolic-C), 133.99 (Ar—C), 132.94 (Ar—C), 132.03 (Ar—C), 131.75 (Phenolic-C), 131.65 (Phenolic-C), 130.28 (Ar—C), 129.37 (Ar—C), 129.16 (4)(Ar—C), 128.41 (Ar—C), 127.88 (Phenolic-C), 127.86 (2)(Ar—C), 126.43 (Phenolic-C & Ar—C), 126.23 (Oxazolone-C=C), 125.90 (Ar—C), 125.88 (Phenolic-C), 124.86 (4)(Phenolic-C & Ar—C), 123.39 (Ar—C), 122.57 (Phenolic-C), 116.55 (CN), 110.40 (Phenolic-C), 86.68 (C—CN). LCMS: calcd. m/z 586.18, found m/z 587.16 [M$^+$]. Anal. calc for: C$_{36}$H$_{22}$N$_6$O$_3$: C, 73.71; H, 3.78; N, 14.33; Found: C, 73.73; H, 3.80; N, 14.31 %.

5-(-(2-hydroxy-3-nitrophenyl)diazenyl)-3-(3-(-(5-oxo-2-phenyloxazol-4(5H)-ylidene)methyl)phenyl)-1-phenyl-1H-pyrazole-4-carbonitrile (7d)

Yield: 86 %. m.p. 60–62 °C. FTIR (KBr, cm^{-1}): 1327 (s, C—N), 1566 (s, N—O), 1681 (s, C=O), 2276 (s, CN), 2924 (w, C—H), 3333 (b, O—H). ^{1}H NMR (500 MHz, DMSO-d_6): δ ppm 10.72 (s, 1H, OH), 8.13 (dd, J = 7.6, 1.4 Hz, 1H, Phenolic Ar—H), 8.01 (dd, J = 7.6, 1.4 Hz, 1H, Phenolic Ar—H), 7.81–7.78 (m, 4H, =CH & Ar—H), 7.53 (s, 3H, Ar—H), 7.41 (d, J = 7.1 Hz, 3H, Ar—H), 7.39–7.23 (m, 5H, Ar—H), 7.18 (s, 1H, Phenolic Ar—H). ^{13}C NMR (100 MHz, DMSO-d_6): δ ppm 166.70 (Oxazolone-C—Ar), 162.01 (C=O), 161.89 (Pyrazole-C—N), 146.98 (C—OH), 142.12 (Phenolic-C), 138.89 (Pyrazole-C=N), 138.83 (Ar—C), 135.84 (=CH), 134.77 (Phenolic-C—NO$_2$), 133.99 (Ar—C), 132.94 (Ar—C), 132.03 (Ar—C), 130.28 (Ar—C), 129.37 (Ar—C), 129.16 (4)(Ar—C), 128.41 (Ar—C), 128.01 (Phenolic-C), 127.88 (2)(Ar—C), 126.87 (Phenolic-C), 126.23 (Oxazolone-C=C), 125.90 (Ar—C), 124.86 (3)(Ar—C), 123.39 (Ar—C), 120.68 (Phenolic-C), 116.55 (CN), 86.68 (C—CN). LCMS: calcd. m/z 581.14, found m/z 582.15 [M$^+$]. Anal. calc for: C$_{32}$H$_{19}$N$_7$O$_5$: C, 66.09; H, 3.29; N, 16.86; Found: C, 66.06; H, 3.31; N, 16.88 %.
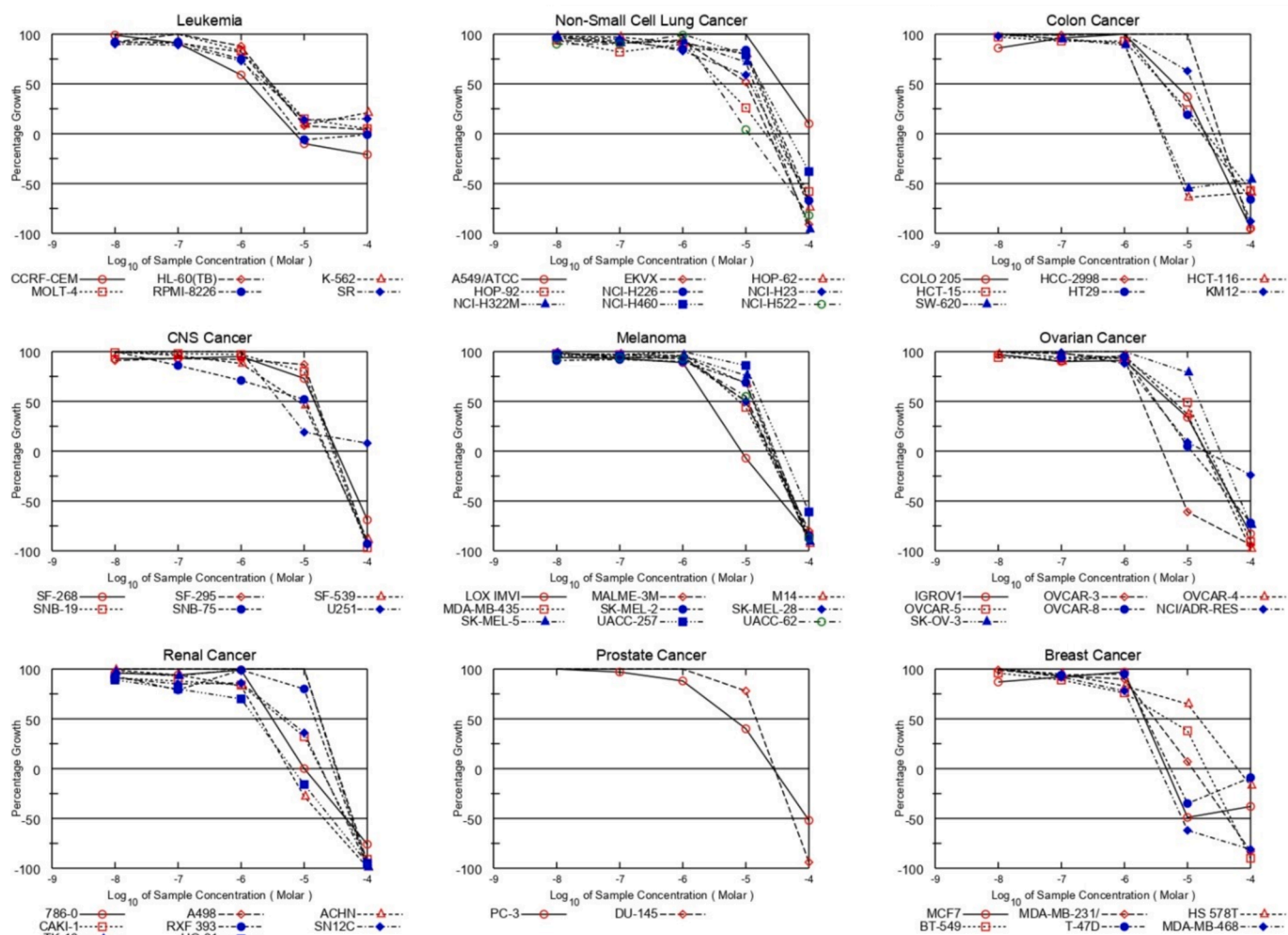
Fig. 4. Graphical presentation of growth inhibition of analogue **7a** at five dose concentrations.

5-(-(2-hydroxy-4-nitrophenyl)diazenyl)-3-(3-(-(5-oxo-2-phenyloxazol-4 (5H)-ylidene)methyl)phenyl)-1-phenyl-1H-pyrazole-4-carbonitrile (7e)

Yield: 91 %. m.p. 260–262 °C. FTIR (KBr, cm^{-1}): 1327 (s, C—N), 1581 (s, N—O), 1689 (s, C=O), 2276 (s, CN), 2916 (w, C—H), 3340 (b, O—H). ^{1}H NMR (500 MHz, DMSO-d_6): δ ppm 9.80 (s, 1H, OH), 8.09 (d, $J = 7.5$ Hz, 1H, Phenolic Ar—H), 7.83–7.74 (m, 6H, =CH & Ar—H), 7.57–7.52 (m, 3H, Ar—H), 7.42–7.38 (d, $J = 7.5$, 1.5 Hz, 2H, Ar—H), 7.33–7.27 (m, 5H, Ar—H), 7.15–7.12 (t, $J = 7.5$, 1.5 Hz, 1H, Ar—H). ^{13}C NMR (100 MHz, DMSO-d_6): δ ppm 166.70 (Oxazolone-C—Ar), 162.01 (C=O), 161.89 (Pyrazole-C—N), 154.42 (C—OH), 150.19 (Phenolic-C—NO$_2$), 141.07 (Phenolic-C), 138.89 (Pyrazole-C=N), 138.82 (Ar—C), 135.84 (=CH), 133.99 (Ar—C), 132.94 (Ar—C), 132.03 (Ar—C), 130.28 (Ar—C), 129.35 (Ar—C), 129.16 (4)(Ar—C), 128.41 (Ar—C), 127.88 (2) (Ar—C), 126.23 (Oxazolone-C=C), 125.90 (Ar—C), 124.86 (3)(Ar—C), 123.39 (Ar—C), 121.57 (Phenolic-C), 116.55 (CN), 116.21 (Phenolic-C), 111.22 (Phenolic-C), 86.68 (C—CN). LCMS: calcd. *m/z* 581.14, found *m/z* 582 [M$^+$]. Anal. calc for: C$_{32}$H$_{19}$N$_7$O$_5$: C, 66.09; H, 3.29; N, 16.86; Found: C, 66.06; H, 3.31; N, 16.88 %.

5-(-(2-hydroxy-5-nitrophenyl)diazenyl)-3-(3-(-(5-oxo-2-phenyloxazol-4 (5H)-ylidene)methyl)phenyl)-1-phenyl-1H-pyrazole-4-carbonitrile (7f)

Yield: 93 %. m.p. 114–116 °C. FTIR (KBr, cm^{-1}): 1327 (s, C—N), 1566 (s, N—O), 1681 (s, C=O), 2276 (s, CN), 2916 (w, C—H), 3333 (b, O—H). ^{1}H NMR (500 MHz, DMSO-d_6): δ ppm 10.32 (s, 1H, OH), 8.90 (d, $J = 1.4$ Hz, 1H, Phenolic Ar—H), 8.08 (dd, $J = 7.6$, 1.4 Hz, 1H, Phenolic

Ar—H), 7.80 (ddd, $J = 13.0$, 3.5, 2.2 Hz, 4H, =CH & Ar—H), 7.76–7.46 (m, 3H, Ar—H), 7.39 (dt, $J = 18.1$, 7.5 Hz, 4H, Ar—H), 7.32–7.21 (m, 3H, Ar—H), 7.19–7.10 (m, 2H, Ar—H). ^{13}C NMR (100 MHz, DMSO-d_6): δ ppm 166.70 (Oxazolone-C—Ar), 163.05 (C—OH), 162.01 (C=O), 161.89 (Pyrazole-C—N), 143.16 (Phenolic-C), 139.72 (Phenolic-C—NO$_2$), 138.89 (Pyrazole-C=N), 138.83 (Ar—C), 135.84 (=CH), 133.99 (Ar—C), 132.94 (Ar—C), 132.03 (Ar—C), 130.28 (Ar—C), 129.37 (Ar—C), 129.16 (4)(Ar—C), 128.41 (Ar—C), 127.88 (2)(Ar—C), 126.44 (Phenolic-C), 126.23 (Oxazolone-C=C), 125.90 (Ar—C), 124.86 (3)(Ar—C), 123.39 (Ar—C), 119.17 (Phenolic-C), 116.65 (Phenolic-C), 116.55 (CN), 86.68 (C—CN). LCMS: calcd. *m/z* 581.14, found *m/z* 582.15 [M + 1]. Anal. calc for: C$_{32}$H$_{19}$N$_7$O$_5$: C, 66.09; H, 3.29; N, 16.86; Found: C, 66.06; H, 3.31; N, 16.88 %.

5-(-(2,4-dihydroxyphenyl)diazenyl)-3-(3-(-(5-oxo-2-phenyloxazol-4 (5H)-ylidene)methyl)phenyl)-1-phenyl-1H-pyrazole-4-carbonitrile (7g)

Yield: 83 %. m.p. 286–288 °C. FTIR (KBr, cm^{-1}): 1296 (s, C—N), 1658 (s, C=O), 2110 (s, CN), 2962 (w, C—H), 3302 (b, O—H). ^{1}H NMR (500 MHz, DMSO-d_6): δ ppm 9.78 (s, 1H, OH), 8.55 (s, 1H, OH), 7.82–7.74 (m, 5H, =CH & Ar—H), 7.39 (m, 3H, Ar—H), 7.31–7.26 (m, 8H, Ar—H), 6.52 (d, $J = 7.5$, 1.5 Hz, 1H, Phenolic Ar—H), 6.47 (s, 1H, Phenolic Ar—H). ^{13}C NMR (100 MHz, DMSO-d_6): δ ppm 166.70 (Oxazolone-C—Ar), 163.76 (C—OH), 162.01 (C=O), 161.89 (Pyrazole-C—N), 160.47 (C—OH), 138.89 (Pyrazole-C=N), 138.83 (Ar—C), 135.84 (=CH), 133.99 (2)(Phenolic-C & Ar—C), 132.94 (Ar—C), 132.03 (Ar—C), 130.28 (Ar—C), 129.37 (Ar—C), 129.16 (4)(Ar—C),
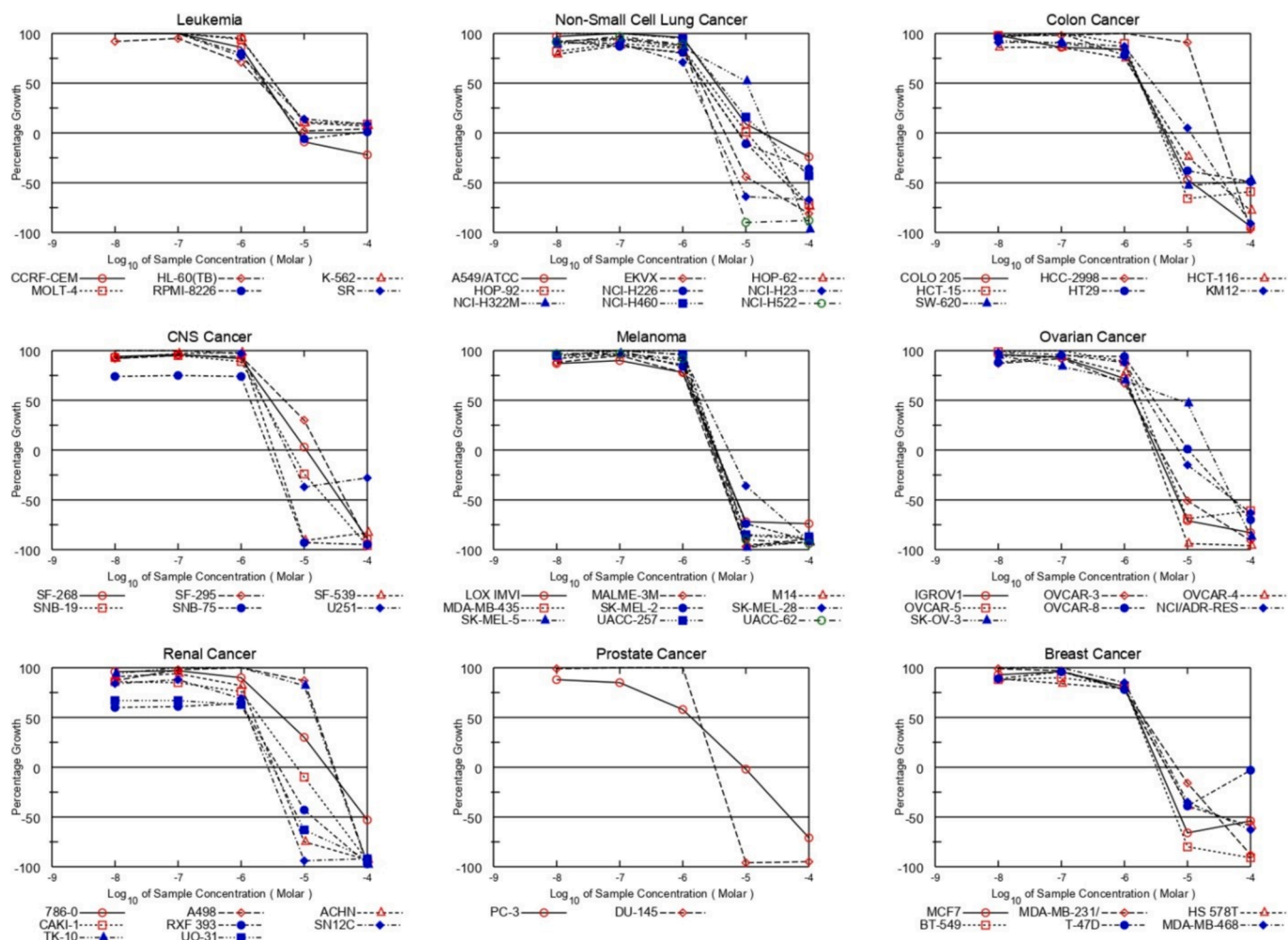
Fig. 5. Graphical presentation of growth inhibition of analogue **7b** at five dose concentrations.

128.41 (Ar—C), 127.88 (2)(Ar—C), 126.20 (Oxazolone-C═C), 125.90 (Ar—C), 124.86 (3)(Ar—C), 124.38 (Phenolic-C), 123.39 (Ar—C), 116.55 (CN), 109.99 (Phenolic-C), 103.13 (Phenolic-C), 86.68 (C—CN). LCMS: calcd. *m/z* 552.15, found *m/z* 553 [M⁺]. Anal. calc for: $C_{32}H_{20}N_6O_4$: C, 69.56; H, 3.65; N, 15.21; Found: C, 69.58; H, 3.63; N, 15.23 %.

5-(-(2,3-dihydroxyphenyl)diazenyl)-3-(3-(-(5-oxo-2-phenyloxazol-4 (5H)-ylidene)methyl)phenyl)-1-phenyl-1H-pyrazole-4-carbonitrile (7h)

Yield: 79 %. m.p. 290–292 °C. FTIR (KBr, cm⁻¹): 1288 (s, C—N), 1651 (s, C═O), 2101 (s, CN), 2746 (w, C—H), 3225 (b, O—H). ¹H NMR (500 MHz, DMSO-*d₆*): δ ppm 9.52 (m, 1H, OH), 7.94 (s, 1H, OH), 7.82–7.52 (m, 7H, ═CH & Ar—H), 7.39–7.32 (m, 3H, Ar—H), 7.29–7.27 (tt, *J* = 6.5, 5.6 Hz, 5H, Ar—H), 7.14–7.12 (ddd, *J* = 8.9, 2.9, 1.4 Hz, 1H, Ar—H), 6.76–6.73 (t, *J* = 7.4 Hz, 1H, Phenolic Ar—H), 6.63–6.61 (dd, *J* = 7.3, 1.4 Hz, 1H, Phenolic Ar—H). ¹³C NMR (100 MHz, DMSO-*d₆*): δ ppm 166.70 (Oxazolone-C—Ar), 162.01 (C═O), 161.89 (Pyrazole-C—N), 146.65 (C—OH), 145.83 (C—OH), 141.45 (Phenolic-C), 138.88 (Pyrazole-C═N), 138.82 (Ar—C), 135.84 (═CH), 133.99 (Ar—C), 132.94 (Ar—C), 132.03 (Ar—C), 130.28 (Ar—C), 129.37 (Ar—C), 129.16 (4)(Ar—C), 128.41 (Ar—C), 127.88 (2)(Ar—C), 126.23 (Oxazolone-C═C), 125.90 (Ar—C), 124.87 (3)(Ar—C), 123.39 (Ar—C), 122.22 (Phenolic-C), 119.14 (Phenolic-C), 116.55 (CN), 113.56 (Phenolic-C), 86.68 (C—CN). LCMS: calcd. *m/z* 552.15, found *m/z* 553.16 [M⁺]. Anal. calc for: $C_{32}H_{20}N_6O_4$: C, 69.56; H, 3.65; N, 15.21; Found: C, 69.58; H, 3.63; N, 15.23 %.

5-(-(5-amino-2-hydroxyphenyl)diazenyl)-3-(3-(-(5-oxo-2-phenyloxazol-4(5H)-ylidene)methyl)phenyl)-1-phenyl-1H-pyrazole-4-carbonitrile (7i)

Yield: 80 %. m.p. 282–284 °C. FTIR (KBr, cm⁻¹): 1319 (s, C—N), 1674 (s, C═O), 2276 (s, CN), 2924 (w, C—H), 3124 (s, N–H), 3225 (b, O—H). ¹H NMR (500 MHz, DMSO-*d₆*): δ ppm 9.26 (s, 1H, OH), 7.82–7.80 (ddd, *J* = 22.4, 3.2, 1.7 Hz, 4H, ═CH & Ar—H), 7.73–7.46 (m, 3H, Ar—H), 7.44–7.36 (m, 2H, Ar—H), 7.36–7.20 (m, 5H, Ar—H), 7.18–7.09 (m, 1H, Ar—H), 7.00 (d, *J* = 1.4 Hz, 1H, Phenolic Ar—H), 6.67 (d, *J* = 7.6 Hz, 1H, Phenolic Ar—H), 6.37 (dd, *J* = 7.6, 1.4 Hz, 1H, Phenolic Ar—H), 4.76 (s, 2H, NH₂). ¹³C NMR (100 MHz, DMSO-*d₆*): δ ppm 166.70 (Oxazolone-C—Ar), 162.00 (C═O), 161.89 (Pyrazole-C—N), 149.80 (C—OH), 142.98 (C—NH₂), 140.78 (Phenolic-C), 138.89 (Pyrazole-C═N), 138.83 (Ar—C), 135.84 (═CH), 133.99 (Ar—C), 132.94 (Ar—C), 132.03 (Ar—C), 130.28 (Ar—C), 129.37 (Ar—C), 129.16 (4)(Ar—C), 128.41 (Ar—C), 127.88 (2)(Ar—C), 126.22 (Oxazolone-C═C), 125.90 (Ar—C), 124.86 (3)(Ar—C), 123.39 (Ar—C), 119.63 (Phenolic-C), 118.61 (Phenolic-C), 116.55 (CN), 108.86 (Phenolic-C), 86.68 (C—CN). LCMS: calcd. *m/z* 551.17, found *m/z* 552.18 [M⁺]. Anal. calc for: $C_{32}H_{21}N_7O_3$: C, 69.68; H, 3.84; N, 17.78; Found: C, 69.65; H, 3.86; N, 17.80 %.

5-(-(2-hydroxy-5-(2-(4-hydroxyphenyl)propan-2-yl)phenyl)diazenyl)-3-(3-(-(5-oxo-2-phenyloxazol-4(5H)-ylidene)methyl)phenyl)-1-phenyl-1H-pyrazole-4-carbonitrile (7j)

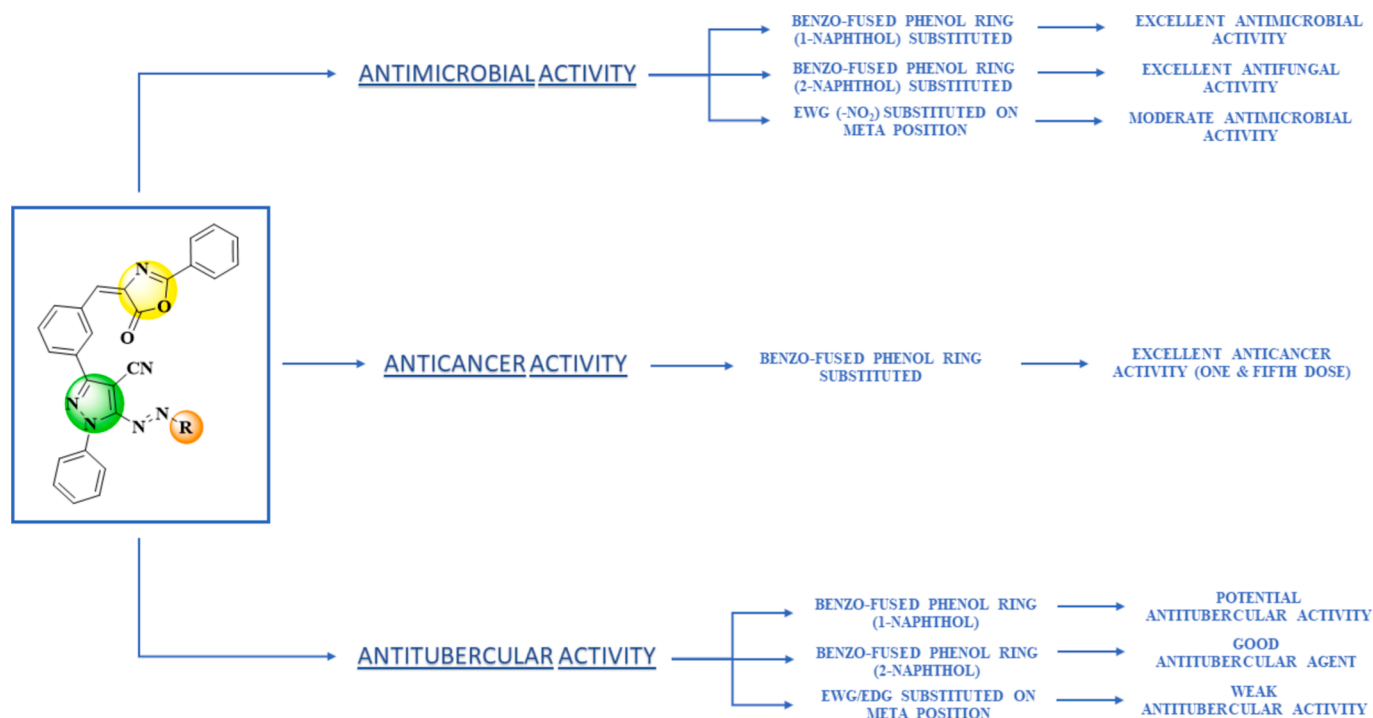Yield: 75 %. m.p. 296–298 °C. FTIR (KBr, cm⁻¹): 1327 (s, C—N),

Fig. 6. SAR for antimicrobial, antitubercular and anticancer activity.

1681 (s, C=O), 2268 (s, CN), 2916 (w, C—H), 3340 (b, O—H). ^{1}H NMR (500 MHz, DMSO-d_6): δ ppm 9.20 (s, 1H, OH), 8.24 (s, 1H, OH), 7.91 (s, 1H, =CH), 7.87 (s, 1H, Phenolic Ar—H), 7.74–7.69 (m, 3H, Ar—H), 7.54–7.53 (d, J = 7.5, 1.5 Hz, 3H, Ar—H), 7.41–7.27 (m, 8H, Ar—H), 7.13 (m, 1H, Ar—H), 7.01–6.93 (d, J = 7.5, 1.5 Hz, 3H, Phenolic Ar—H), 6.71 (d, J = 7.5, 1.5 Hz, 2H, Phenolic Ar—H), 1.71 (s, 6H, CH$_3$); ^{13}C NMR (100 MHz, DMSO-d_6): δ ppm 166.70 (Oxazolone-C—Ar), 162.01 (C=O), 161.89 (Pyrazole-C—N), 154.57 (C—OH), 152.27 (C—OH), 142.42 (Phenolic-C), 141.44 (Phenolic-C), 138.89 (Pyrazole-C=N), 138.83 (Ar—C), 137.65 (Phenolic-C), 135.84 (=CH), 133.88 (2) (Phenolic-C & Ar—C), 132.94 (Ar—C), 132.03 (Ar—C), 130.28 (Ar—C), 129.37 (Ar—C), 129.16 (4)(Ar—C), 128.41 (Ar—C), 128.20 (2) (Phenolic-C), 127.88 (2)(Ar—C), 126.23 (Oxazolone-C=C), 125.90 (Ar—C), 124.86 (3)(Ar—C), 123.39 (Ar—C), 119.80 (Phenolic-C), 116.56 (3)(CN & Phenolic-C), 114.53 (Phenolic-C), 86.68 (C—CN), 46.39 (C—CH$_3$), 30.33 (2)(CH$_3$). LCMS: calcd. m/z 670.23, found m/z 671 [M$^+$]. Anal. calc for: C$_{41}$H$_{30}$N$_6$O$_4$: C, 73.42; H, 4.51; N, 12.53; Found: C, 73.45; H, 4.49; N, 12.55 %.

Antimicrobial assay

To identify antimicrobial activity, the Mueller Hinton Broth dilution method of minimum inhibitory concentration (MIC) was used on a range of microorganisms. These include *E. coli* (MTCC-443), *P. aeruginosa* (MTCC-1688), *S. aureus* (MTCC-96) and *S. pyogenes* (MTCC-442) Gram-strain bacteria's and fungi including *C. albicans* (MTCC-227), *A. niger* (MTCC-282), and *A. clavatus* (MTCC-1323). Compounds **(7a–j)** were tested against these strains at concentrations of 1000, 500, and 250 μg/mL in the initial screening. The active compounds were further evaluated by diluting them and observing their development after one or two days at concentrations of 62.5, 50, 25, and 12.5 μg/mL. Chloramphenicol, ciprofloxacin, and norfloxacin were utilized as the standard drugs to evaluate the antibacterial activity and nystatin and griseofulvin to assess antifungal potency [39,40].

Antitubercular and cytotoxicity assay

Synthesized motifs **(7a–j)** were tested for their ability to kill *Mycobacterium tuberculosis* H$_{37}$Rv strain in BACTEC 12B medium. This was done using the microplate alamar blue assay (MABA) at a concentration of 6.25 μg/mL. In the first stage, compounds that inhibited the bacteria by 90 % or more were examined again at and below 6.25 μg/mL to identify the minimum inhibitory concentration (MIC). The compounds also tested for their cytotoxic properties in VERO cells at concentrations less than or equal to 62.5 μg/mL or 10 times the MIC for *M. tuberculosis* H$_{37}$Rv. After 72 h, the cells' viability was assessed using the Promega CellTiter 96 Non-radioactive Cell Proliferation Assay, which converts MTT into a formazan product. Finally, the selectivity index (SI) has been calculated using the standard formula: IC$_{50}$/MIC. An SI greater than 10 was considered significant [41].

Anticancer screening assay

The Anticancer screening process was assessed by the Developmental Therapeutics Program (DTP) at the National Cancer Institute located in Bethesda, USA. In the initial stage of screening, all compounds **(7a–j)** were tested against 60 cell lines at a single dose of 10^{-5} M. The 60 human cancer cell lines were categorized into nine subpanels, each representing a different human cancer type, including Leukemia, Non-Small Cell Lung Cancer, Colon, CNS, Melanoma, Ovarian, Renal, Prostate, and Breast Cancer cell lines. The COMPARE application was used to analyze the mean graph obtained from the initial stage screening, following the protocol described in the literature [42,43]. "Compounds were tested against the 60-cell panel at five different concentration levels if they significantly limit growth. The human tumor cell lines in the cancer screening panel have been maintained in RPMI 1640 media outlets containing 5 % fetal bovine serum and 2 mm L-glutamine. Cells were injected into 96-well microliter plates in 100 μl at plating densities ranging from 5000 to 40,000 cells/well, depending on the doubling time of different cell lines for a typical screening experiment. Prior to introducing experimental drugs, microscope plates were incubated for a full day at 37 °C, 5 % CO$_2$, 95 % air, and 100 % moisture content after cell

inoculation.

To reflect the count of the cell population for each cell line at the moment of drug administration (Tz), two plates of each cell line were fixed in situ with TCA after 24 h. Prior to usage, experimental medicines were stored frozen after being dissolution in dimethyl sulfoxide at 400 times the intended final maximum test concentration. An aliquot of frozen concentrate was defrosted before being mixed with an entirety of medium containing 50 μg/ml gentamicin, which proceeds to dilute to twice the desired final maximum test concentration. For the purpose of obtaining a total of five drug concentrations plus control, additional four-, ten-fold-, or half-log dilutions in sequence were made. The remainder of 100 μl of each of these dosage preparations was added into the appropriate microliter boreholes, which typically hold 100 μl liquid substrate, yielding in the needed final drug contents.

Upon the infusion of the medicine, the plates were incubated for two days at 37 °C, 5 % CO_2, 95 % air, and absolute humidity of one hundred percent. The assay for following cells was ended by the addition of cold TCA. Cells were fixed in place by gently adding 50 μl of cool 50 % (w/v) 10 % TCA and incubating at 4 °C for 60 min. The supernatant was discarded, and the plates were rinsed and air dried five times with tap water. Sulforhodamine B (SRB) solution (100 μl) at 0.4 % (w/v) in 1 % acetic acid was added to each well, and plates were incubated at room temperature for 10 min. Following staining, unbound dye was removed by washing the plates five times with 1 % acetic vinegar and air drying them. The bound dye was then solubilized with 10 mm trizma base, and the absorbance was measured using an automated plate reader at 515 nm. The protocol was the same for suspension cells, except that the test was concluded by gradually injecting 50 μl of 80 % TCA with 16 % final concentration to fix getting settled cells at the bottom of the wells. The percentage growth could have estimated at each of the drug concentration levels using the seven absorbance measurements [time zero, (Tz), control growth, (C), and testing expansion for the presence of drug at the five concentration levels (Ti)]. The growth inhibition percentage is computed as:

$$[(Ti - Tz)/(C - Tz)] \times 100 \text{ for concentration for which } Ti >/= Tz$$
$$[(Ti - Tz)/Tz] \times 100 \text{ for concentration for which } Ti < Tz$$

For each experimental drug, three dose–response parameters were computed. The drug dose resulting in a 50 % reduction in the net protein growth (as determined by SRB staining) in control cells during drug incubation was computed as $[(Ti - Tz)/(C - Tz)] \times 100 = 50$. $Ti = Tz$ was used to calculate the medication concentration that results in all growth restriction (TGI). The LC_{50} (drug concentration resulting in a 50 % drop in measured protein at the last stage of a course of treatment relative to the beginning) indicating an overall reduction of cells subsequent intervention was calculated as $[(Ti - Tz)/Tz] \times 100 = 50$. Values were determined for all of these three variables if a certain amount of activity has been achieved; if the impact fails to occur or exceeds the level of activity, the value for that variable can be defined as either more or less than the greatest or smallest level tested.

Data retrieval and preparation

The 3D structures of bacterial targets such as CusC (PDB ID: 3PIK), Multidrug efflux pump submit AcrB (PDB ID: 4U8V), MexABOprM (PDB ID: 6IOL), TriABC (PDB ID: 6VEJ), Cadmium efflux system accessory protein (PDB ID: 1U2W), Multidrug Efflux Pump MepR (PDB ID: 4LLL), Tagatose-1,6-bisphosphate aldolase (PDB ID: 5F2M), Streptopain (PDB ID: 6UQD); fungal targets such as Serine/Threonine phosphatase Z1 (PDB ID: 5JPF), Sterol 14-alpha demethylase (PDB ID: 5TZ1), Chitinase B (PDB ID: 6IGY), Prolyl endoprotease (PDB ID: 7WAB), Spherulin-4 (PDB ID: 5D6T), M36 protease (PDB ID: 7Z6T); *M.tb.* targets such as Enoyl-[acyl-carrier-protein] reductase (PDB ID: 6GH1), and Topoisomerase I (PDB ID: 6CQI) were retrieved from Protein Data Bank database respectively [44]. The excess chains, water molecules and bound ligands were removed and the protein were prepared for docking. The 3-D structures of compounds such as Chloramphenicol (PubChem ID: 5959), Ciprofloxacin (PubChem ID: 2764), Norfloxacin (PubChem ID: 4539), Nystatin (PubChem ID: 6433272), Griseofulvin (PubChem ID: 441140), Isoniazid (PubChem ID: 3767) were retrieved from PubChem database respectively [45]. In addition, the smiles of the compounds **7b**, **7c** and **7e** were predicted by Chemdraw and their respective 3D structures were retrieved using Open Babel. Furthermore, their energies were minimized and prepared for the docking studies.

Molecular docking

The binding affinities of the selected hit compounds were tested against various bacterial, fungal, and tuberculosis targets through AutoDock Vina [46,47]. The prepared protein receptors were visualized to identify the suitable pockets on their surface and then the grid box was set at their respective pockets of each targets. A grid box of 25 × 25 × 25 dimensions were set in X, Y, and Z directions, and the point spacing was set as 0.375 Å. Also, the Kollman charges were added and Lamarckinan genetic algorithm was selected for the docking study. Then the runs were set as 10 and all the other parameters were kept default. Finally, the docked complexes of the receptor-ligand complex, and the interaction between them were visualized by Discovery studio visualizer.

CRediT authorship contribution statement

Bonny Y. Patel: Writing – review & editing, Supervision, Methodology, Investigation, Conceptualization. **Vidhi Joshi:** Writing – original draft, Investigation. **Sangeetha Subramanian:** Writing – review & editing, Supervision, Investigation. **Gopal Italiya:** Writing – original draft, Visualization, Investigation. **Prasanna Srinivasan Ramalingam:** Writing – review & editing, Software. **Sivakumar Arumugam:** Writing – review & editing, Software, Methodology. **Sanjay D. Hadiyal:** Methodology, Investigation, Formal analysis. **Al-Anood Mohamed Al-Dies:** Visualization, Investigation, Formal analysis.

Declaration of competing interest

The authors declare that they have no known competing financial interests or personal relationships that could have appeared to influence the work reported in this paper.

Appendix A. Supplementary material

Supplementary data to this article can be found online at https://doi.org/10.1016/j.rechem.2024.101887.

Data availability

Supporting Information (Figs. S1–S42): Full experimental detail, FTIR, LCMS, ^{1}H and ^{13}C NMR spectra as well as anticancer study graphs. This material can be found via the "Supplementary Content" section of this article's webpage.

References

[1] G. Annunziato, Strategies to overcome antimicrobial resistance (AMR) making use of non-essential target inhibitors: a review, Int. J. Mol. Sci. 20 (2019) 5844, https://doi.org/10.3390/ijms20235844.

[2] S. Tiberi, M. Muñoz-Torrico, R. Duarte, M. Dalcolmo, L. D'Ambrosio, G.B. Migliori, New drugs and perspectives for new anti-tuberculosis regimens, Pulmonology 24 (2018) 86–98, https://doi.org/10.1016/j.rppnen.2017.10.009.

[3] O. Ebenezer, M.A. Jordaan, G. Carena, T. Bono, M. Shapi, J.A. Tuszynski, An Overview of the biological evaluation of selected nitrogen-containing heterocycle medicinal chemistry compounds, Int. J. Mol. Sci. 23 (2022) 8117, https://doi.org/10.3390/ijms23158117.

[4] A.P. Taylor, R.P. Robinson, Y.M. Fobian, D.C. Blakemore, L.H. Jones, O. Fadeyi, Modern advances in heterocyclic chemistry in drug discovery, Org. Biomol. Chem. 14 (2016) 6611–6637, https://doi.org/10.1039/C6OB00936K.

[5] J.S. Fisk, R.A. Mosey, J.J. Tepe, The diverse chemistry of oxazol-5-(4*H*)-ones, Chem. Soc. Rev. 36 (2007) 1432–1440, https://doi.org/10.1039/B511113G.

[6] D.S.A. Haneen, W.S.I. Abou-Elmagd, A.S.A. Youssef, 5(4*H*)-oxazolones: synthesis and biological activities, Synth. Commun. 51 (2020) 215–233, https://doi.org/10.1080/00397911.2020.1825746.

[7] A.A. Deshpande, R.A. Gossage, S.M. Jackson, J.W. Quail, A.L. Sadowy, P.N. Yadav, An exploration of the metal oxide-assisted decomposition and rearrangement of *N*-Acyl-1,3-oxazolidin-2-ones leading to 2-aryl-2-oxazolines [1], Z. Naturforsch. 64b (2009) 1046–1052.

[8] P.N. Yadav, R.A. Gossage, A. Decken, Crystal structure of *trans*-Bis[2-(*p*-fluorophenyl)-2-oxazoline-*k*¹*N*]platinum(II) dichloride], Anal. Sci. 24 (2008) x301.

[9] A. Decken, L. Botelho, A.L. Sadowy, P.N. Yadav, R.A. Gossage, 2-(3-Nitro-phen-yl)-2-oxazoline, Acta Cryst. E 62 (2006) o5414–o5416, https://doi.org/10.1107/S1600536806045454.

[10] M.A. Zolfigol, F. Afsharnadery, S. Baghery, S. Salehzadeh, F. Maleki, Catalytic applications of {[HMIM]C(NO2)3}: as a nano ionic liquid for the synthesis of pyrazole derivatives under green conditions and a mechanistic investigation with a new approach, RSC Adv. 5 (92) (2015) 75555–75568, https://doi.org/10.1039/C5RA16289K.

[11] A.R. Farghaly, S.A. Ahmed, K.S. Ismail, D. Ibrahim, N. Amri, S. Elgogary, Synthesis, antitumor activity, antimicrobial evaluation and molecular docking studies of some hydrazone, 1,3,4-oxadiazole, 1,2,4-triazole and pyrazole derivatives bearing nicotinoyl moiety, Results Chem 7 (2024) 101474, https://doi.org/10.1016/j.rechem.2024.101474.

[12] N.C. Desai, B.Y. Patel, B.P. Dave, Approach for the synthesis of potent antimicrobials containing pyrazole, pyrimidine and morpholine analogues, Int. Lett. Chem. Phys. Astron. 69 (2016) 87–96, https://doi.org/10.18052/www.scipress.com/ILCPA.69.87.

[13] H.D. Trivedi, V.B. Joshi, B.Y. Patel, Pyrazole bearing pyrimidine analogues as the privileged scaffolds in antimicrobial drug discovery: a review, Anal. Chem. Lett. 12 (2022) 147–173, https://doi.org/10.1080/22297928.2021.1910565.

[14] R. Kuranea, S. Khanapurea, D. Kalea, R. Salunkhea, G. Rashinkara, An expedient synthesis of oxazolones using cellulose supported ionic liquid phase catalyst, RSC Adv. 6 (50) (2016) 44135–44144, https://doi.org/10.1039/C6RA03873E.

[15] H.D. Trivedi, B.Y. Patel, P.K. Patel, S.R. Sagar, Synthesis, molecular modeling, ADMET and fastness studies of some quinoline encompassing pyrimidine azo dye derivatives as potent antimicrobial agents, Chem. Data Coll. 41 (2022) 100923, https://doi.org/10.1016/j.cdc.2022.100923.

[16] A.G. Prashantha, J. Keshavayya, R.A. Shoukat Ali, Synthesis, spectral characterizations and biological applications of novel 3-[(E)-(4, 6-dihydroxy pyrimidin-5-yl)diazenyl]-4-methylbenzoic acid azo Dye and their derivatives, Results Chem. 3 (2021) 100110, https://doi.org/10.1016/j.rechem.2021.100110.

[17] K. Mezgebe, E. Mulugeta, Synthesis and pharmacological activities of azo dye derivatives incorporating heterocyclic scaffolds: a review, RSC Adv. 12 (2022) 25932–25946, https://doi.org/10.1039/D2RA04934A.

[18] M.N. Khan, D.K. Parmar, D. Das, Recent applications of azo dyes: a paradigm shift from medicinal chemistry to biomedical sciences, Mini-Rev. Med. Chem. 21 (2021) 1071–1084, https://doi.org/10.2174/1389557520999201123210025.

[19] Y. Ali, S.A. Hamid, U. Rashid, Biomedical applications of aromatic azo compounds, Mini-Rev. Med. Chem. 18 (2018) 1548–1558, https://doi.org/10.2174/1389557518666180524113111.

[20] H.D. Trivedi, B.Y. Patel, S.D. Hadiyal, G. Italiya, P.S. Ramalingam, A green one-pot synthetic protocol of hexahydropyrimido[4,5-*d*]pyrimidin-4(1*H*)-one derivatives: molecular docking, ADMET, anticancer and antimicrobial studies, Mol. Divers. 28 (2024) 183–195, https://doi.org/10.1007/s11030-023-10712-9.

[21] N.C. Desai, N. Bhatt, A. Dodiya, T. Karkar, B. Patel, M. Bhatt, Synthesis, characterization and antimicrobial screening of thiazole based 1,3,4-oxadiazoles heterocycles, Res. Chem. Intermed. 42 (2016) 3039–3053, https://doi.org/10.1007/s11164-015-2196-x.

[22] H.D. Trivedi, V.B. Joshi, B.Y. Patel, Water mediated pot, atom, and step economic (PASE) synthesis of pyrimido[4,5-*d*]pyrimidines using ultrasound and microwave irradiation approaches, Synth. Commun. 53 (2023) 823–834, https://doi.org/10.1080/00397911.2023.2199358.

[23] N.C. Desai, J.P. Harsora, B.Y. Patel, K.A. Jadeja, Synthesis of a novel series of imines containing nitrogen heterocycles as promising antibacterial and antifungal agents, Indian J. Chem. B 56B (2017) 976–983. http://nopr.niscpr.res.in/handle/123456789/42721.

[24] N.C. Desai, H.V. Vaghani, B.Y. Patel, T.J. Karkar, Synthesis and antimicrobial activity of fluorine containing pyrazole-clubbed dihydropyrimidinones, Indian J. Pharm. Sci. 80 (2) (2018) 242–252, https://doi.org/10.4172/PHARMACEUTICAL-SCIENCES.1000351.

[25] N.C. Desai, M.R. Pandya, B.Y. Patel, M.J. Bhatt, T.J. Karkar, Synthesis of novel N, N-dimethyl-1-(5-methyl-2-arylimidazo[1,2-a]pyridin-3-yl)methanamine derivatives as potential antimicrobial agents, Indian J. Chem. b. 55B (2016) 1136–1143. http://nopr.niscpr.res.in/handle/123456789/35365.

[26] H.D. Trivedi, V.B. Joshi, B.Y. Patel, Quinoline incorporating pyrimidine heterocyclic azo dye derivatives: synthesis, characterization and applications, Indian J. Chem. 62 (2023) 380–392, https://doi.org/10.56042/ijc.v62i4.425.

[27] N.C. Desai, B.Y. Patel, K.A. Jadeja, B.P. Dave, Landscaping of quinoline based heterocycles as potential antimicrobial agents: a mini review, Nov. Appro. Drug Des. Dev. 1 (2017) 555–570, https://doi.org/10.19080/NAPDD.2017.01.555570.

[28] J.R. Mekala, R.K. Kurappalli, P. Ramalingam, N.R. Moparthi, N-acetyl l-aspartate and Triacetin modulate tumor suppressor MicroRNA and class I and II HDAC gene expression induce apoptosis in Glioblastoma cancer cells in vitro, Life Sci. 286 (2021) 120024, https://doi.org/10.1016/j.lfs.2021.120024.

[29] J.R. Mekala, P.S. Ramalingam, S. Mathavan, R.B.R.D. Yamajala, N.R. Moparthi, R.K. Kurappalli, R.R. Manyam, Synthesis, in vitro and structural aspects of cap substituted Suberoylanilide hydroxamic acid analogs as potential inducers of apoptosis in Glioblastoma cancer cells via HDAC/microRNA regulation, Chem-Biol. Interact. 357 (2022) 109876, https://doi.org/10.1016/j.cbi.2022.109876.

[30] D. Chen, N. Oezguen, P. Urvil, C. Ferguson, S.M. Dann, T.C. Savidge, Regulation of protein-ligand binding affinity by hydrogen bond pairing, Sci. Adv. 2 (2016) e1501240, https://doi.org/10.1126/sciadv.1501240.

[31] A. Shah, N. Teraiya, J.H. Kamdar, T. Juneja, C.B. Sangani, S. Ahmed, K. Kapadiya, Novel purine derivatives as selective CDK2 inhibitors with potential anticancer activities: design, synthesis and biological evaluation, Bioorg. Chem. 153 (2024) 107841, https://doi.org/10.1016/j.bioorg.2024.107841.

[32] D. Yevale, N. Teraiya, T. Lalwani, M. Dalasaniya, K. Kapadiya, R.K. Ameta, C.B. Sangani, Y.-T. Duan, PI3Kδ and mTOR dual inhibitors: design, synthesis and anticancer evaluation of 3-substituted aminomethylquinoline analogues, Bioorg. Chem. 147 (2024) 107323, https://doi.org/10.1016/j.bioorg.2024.107323.

[33] A.A. Bhat, N. Tandon, I. Singh, R. Tandon, Structure-activity relationship (SAR) and antibacterial activity of pyrrolidine based hybrids: a review, J. Mol. Struct. 1283 (2023) 135175, https://doi.org/10.1016/j.molstruc.2023.135175.

[34] Z. Xu, C. Gao, Q.-C. Ren, X.-F. Song, L.-S. Feng, Z.-S. Lv, Recent advances of pyrazole-containing derivatives as anti-tubercular agents, Eur. J. Med. Chem. 139 (2017) 429–440, https://doi.org/10.1016/j.ejmech.2017.07.059.

[35] S. Joshi, M. Mehra, R. Singh, S. Kakar, Review on chemistry of oxazole derivatives: current to future therapeutic prospective, Egypt. J. Basic Appl. Sci. 10 (1) (2023) 218–239, https://doi.org/10.1080/2314808X.2023.2171578.

[36] N.C. Desai, A.S. Maheta, K.M. Rajpara, V.V. Joshi, H.V. Vaghani, H.M. Satodiya, Green synthesis of novel quinoline based imidazole derivatives and evaluation of their antimicrobial activity, J. Saudi Chem. Soc. 18 (6) (2014) 963–971, https://doi.org/10.1016/j.jscs.2011.11.021.

[37] N. Singh, J. Pandey, DABCO catalyzed, green and efficient, one-pot multicomponent synthesis of 5-aminopyrazole-4-carbonitrile, Curr. Res. Green Sustain. Chem. 4 (2021) 100134, https://doi.org/10.1016/j.crgsc.2021.100134.

[38] S. Benkhaya, S. M'rabet, A. El Harfi, Classifications, properties, recent synthesis and applications of azo dyes, Heliyon 6 (1) (2020) e03271, https://doi.org/10.1016/j.heliyon.2020.e03271.

[39] N.C. Desai, B.Y. Patel, B.P. Dave, Synthesis and antimicrobial activity of novel quinoline derivatives bearing pyrazoline and pyridine analogues, Med. Chem. Res. 26 (2017) 109–119, https://doi.org/10.1007/s00044-016-1732-6.

[40] R.V. Aghara, M.C. Parmar, B.Y. Patel, Synthesis of pyridine clubbed tetrahydrobenzo[*b*]thiophene azo dye analogues using the Gewald reaction: catalytic optimization, antibacterial, and dye investigation, Russ. J. Gen. Chem. 93 (2023) 2393–2403, https://doi.org/10.1134/S1070363223090207.

[41] B.Y. Patel, T.J. Karkar, M.J. Bhatt, Synthesis of 5-substituted-1,3,4-oxadiazole clubbed pyrazole and dihydropyrimidine derivatives as potent bioactive agents, Eur. Chem. Bull. 10 (2021) 13–20, https://doi.org/10.17628/ecb.2021.10.13-20.

[42] N. Ramani, B.Y. Patel, G. Italiya, P.S. Ramalingam, R. Mishra, S. Subramanian, S. D. Hadiyal, Synthesis of 8-methyl-2-phenylquinazolin-4(3*H*)-ones derived Schiff's bases: spectroscopic properties, SAR, docking approaches and their anticancer and antimicrobial activity, J. Mol. Struct. 1310 (2024) 138256, https://doi.org/10.1016/j.molstruc.2024.138256.

[43] M.N. Noolvi, H.M. Patel, Synthesis, method optimization, anticancer activity of 2,3,7-trisubstituted quinazoline derivatives and targeting EGFR-tyrosine kinase by rational approach: 1st cancer update, Arab. J. Chem. 6 (2013) 35–48, https://doi.org/10.1016/j.arabjc.2010.12.031.

[44] S.K. Burley, C. Bhikadiya, C. Bi, S. Bittrich, H. Chao, L. Chen, P.A. Craig, G. V. Crichlow, K. Dalenberg, J.M. Duarte, S. Dutta, M. Fayazi, Z. Feng, J.W. Flatt, S. Ganesan, S. Ghosh, D.S. Goodsell, R.K. Green, V. Guranovic, J. Henry, B. P. Hudson, I. Khokhriakov, C.L. Lawson, Y. Liang, R. Lowe, E. Peisach, I. Persikova, D.W. Piehl, Y. Rose, A. Sali, J. Segura, M. Sekharan, C. Shao, B. Vallat, M. Voigt, B. Webb, J.D. Westbrook, S. Whetstone, J.Y. Young, A. Zalevsky, C. Zardecki, RCSB Protein Data Bank (RCSB.org): delivery of experimentally-determined PDB structures alongside one million computed structure models of proteins from artificial intelligence/machine learning, Nucleic Acids Res. 51 (2023) D488–D508, https://doi.org/10.1093/nar/gkac1077.

[45] S. Kim, J. Chen, T. Cheng, A. Gindulyte, J. He, S. He, Q. Li, B.A. Shoemaker, P. A. Thiessen, B. Yu, L. Zaslavsky, J. Zhang, E.E. Bolton, PubChem in 2021: new data

content and improved web interfaces, Nucleic Acids Res. 49 (2021) (2021) D1388–D1395, https://doi.org/10.1093/nar/gkaa971.

[46] O. Trott, A.J. Olson, AutoDock Vina: improving the speed and accuracy of docking with a new scoring function, efficient optimization, and multithreading, J. Comput. Chem. 31 (2009) 455–461, https://doi.org/10.1002/jcc.21334.

[47] P.S. Ramalingam, P. Balakrishnan, S. Rajendran, A. Jothi, R. Ramalingam, S. Arumugam, Identification of dietary bioflavonoids as potential inhibitors against KRAS G12D Mutant—novel insights from computer-aided drug discovery, Curr. Issues Mol. Biol. 45 (2023) 2136–2156, https://doi.org/10.3390/cimb45030137.